



The AWAKEN wind farm benchmark, Part 2: Modeling results

Nicola Bodini¹, Patrick Moriarty¹, Regis Thedin¹, Paula Doubrawa², Cristina Archer³, Myra Blaylock⁴, Carlo Bottasso⁵, Bruno Carmo⁶, Lawrence Cheung⁴, Camille Dubreuil⁷, Rogier Floors⁸, Thomas Herges⁴, Daniel Houck⁴, Ali Kanjari³, Colleen M. Kaul⁹, Christopher Kelley⁴, Ru LI¹⁰, Julie K. Lundquist^{11,1}, Desirae Major⁵, Anh Kiet Nguyen⁷, Mike Optis¹², Luan R. C. Parada⁶, Alfredo Peña⁸, Julian Quick⁸, David Ricarte⁶, William C. Radünz^{6,11}, Raj K. Rai⁹, Oscar Garcia Santiago⁸, Jonas Schulte¹³, Knut S. Seim⁷, M. Paul van der Laan⁸, Kisorthman Vimalakanthan¹⁴, and Adam Wise^{15,16}

¹National Laboratory of the Rockies, Golden, CO, United States of America

²WSP USA Inc., Boulder, CO, United States of America

³University of Delaware, Newark, DE, United States of America

⁴Sandia National Laboratories, Albuquerque, NM, and Livermore, CA, United States of America

⁵Technical University of Munich, Munich, Germany

⁶University of São Paulo, São Paulo, Brazil

⁷Equinor, Sandsli, Norway

⁸Technical University of Denmark, Roskilde, Denmark

⁹Pacific Northwest National Laboratory, Richland, WA, United States of America

¹⁰Meteodyn, Saint-Herblain, France

¹¹Johns Hopkins University, Baltimore, MD, United States of America

¹²Veer Renewables, Courtenay, British Columbia, Canada

¹³Fraunhofer IWES, Bremerhaven, Germany

¹⁴TNO, EMT Unit, Petter, Netherlands

¹⁵University of California, Berkeley, CA, United States of America

¹⁶Lawrence Livermore National Laboratory, Livermore, CA, United States of America

Correspondence: Nicola Bodini (nicola.bodini@nlr.gov)

Abstract. Accurately modeling wind farm performance in complex atmospheric flows remains a challenge. This paper presents the modeling results of the American WAKE experiment (AWAKEN) wind farm benchmark, a collaborative effort involving 16 research groups from academia and industry within the International Energy Agency Wind Technology Collaboration Programme Task 57. The study evaluates a diverse suite of simulation tools, ranging from fast-running engineering wake models to high-fidelity large-eddy simulations, against a diurnal case study observed during the AWAKEN campaign. The benchmark utilized a three-phase structure to progressively assess model performance as observational data availability increased. Initial blind predictions showed that higher-fidelity models did not uniformly outperform simpler simulation tools. A distinct spatial bias was observed where models struggled to resolve the interplay between a low-level jet, wakes, and terrain-induced flow acceleration. In subsequent phases, leveraging additional measurements for model improvement led to a reduction in mean absolute error across the model ensemble; however, this effect was most pronounced in engineering wake models, where targeted calibration reduced error by up to 40 %. Overall, the study demonstrates that inflow characterization remains a primary prerequisite for accuracy, particularly for models relying on coarse forcing datasets. While the limited ability to resolve local



terrain-flow interactions under single-day conditions represent a recognized constraint, the overall findings on wake modeling and real-world validation still provide valuable guidance for model application and for mitigating this limitation.

- 15 *Copyright statement.* This work was authored in part by the National Laboratory of the Rockies for the U.S. Department of Energy (DOE),
operated under Contract No. DE-AC36-08GO28308. Funding provided by U.S. Department of Energy Office of Energy Efficiency and
Renewable Energy Wind Energy Technologies Office. The views expressed in the article do not necessarily represent the views of the DOE
or the U.S. Government. The U.S. Government retains and the publisher, by accepting the article for publication, acknowledges that the U.S.
Government retains a nonexclusive, paid-up, irrevocable, worldwide license to publish or reproduce the published form of this work, or allow
20 others to do so, for U.S. Government purposes.

1 Introduction

Building on the characterization of the atmospheric and operational conditions presented in the companion Part 1 paper (Bodini
et al., in review), here we focus on the modeling component of the American WAKE experimeNt (AWAKEN) wind farm
benchmark, which represents the first benchmarking exercise within the International Energy Agency (IEA) Wind Technology
25 Collaboration Programme Task 57. The benchmark brings together a diverse set of modeling approaches, from engineering
wake models to mesoscale–microscale coupled frameworks and large-eddy simulation (LES), to evaluate how well current
tools reproduce the observed wind flow, wake behavior, and turbine impacts documented during the selected case study.

The complexity of this task is underscored by recent benchmarking efforts that have sought to quantify model uncertainty and
bias across different scales. At the single-turbine scale, results from the SWiFT site (Doubrawa et al., 2020) demonstrated that
30 while model performance generally tracks with fidelity in neutral conditions, steady-state Reynolds-averaged Navier–Stokes
(RANS) simulations can outperform higher-fidelity tools in stable conditions due to the ease of prescribing non-canonical in-
flows. On a larger scale, an evaluation of 19 offshore wind farms (Nygaard et al., 2022) established a wake model uncertainty of
less than 10% for models accounting for global blockage and heterogeneous flow. However, that study also revealed systematic
limitations in traditional engineering tools: the standard Park model (Jensen, 1983) tends to underestimate wake losses and
35 overestimate wind speed recovery as turbine spacing increases. While newer models like TurbOPark (Pedersen et al., 2022)
have shown lower bias across varying spacings offshore, their applicability to complex land-based environments—where time-
dependent turbulence and diurnal cycles dominate—remains largely untested.

Comparing models across such a broad spectrum of fidelity and complexity thus presents unique challenges. Beyond the
physical representation of atmospheric stability and turbine parameterization, the "human factor"—subjective decisions made
40 by modelers regarding grid setup, spin-up times, and mesh refinement—adds a significant layer of uncertainty. To disentangle
these factors, this benchmark adopts a multiphase blind approach. By progressively releasing observational data (Sect. 2),
we track not only the baseline performance of state-of-the-art tools but also their ability to adapt and improve via model
calibration. Section 3 details the diverse participating models and their setup evolution through the phases. Section 4 presents



the comparative results, analyzing bias, error spatial distribution, and wake-specific metrics. Finally, Sect. 5 summarizes the
45 scientific and operational lessons learned from this extensive international exercise.

2 Structure of the benchmark

This benchmark was designed to evaluate how well different modeling approaches capture key aspects of wind farm behavior
under real-world conditions, a key goal of IEA Task 57. These include the representation of inflow characteristics, wake
behavior at both the turbine and farm scales, impacts on downstream farms, and, ultimately, power production. To encourage
50 broad participation and comparison, the benchmark welcomed a wide range of simulation tools, from mesoscale models with
varying parameterizations to analytical and engineering models and higher-fidelity approaches such as LES and RANS models.

We structured the benchmark into three phases:

- Phase 1: the baseline. The purpose of this phase was to replicate industry practice, where an analyst must estimate
energy production based on limited observations at a site. The benchmark team released limited inflow observations
55 for 24 August 2023 (and the previous day, in case they were needed to initialize simulations), along with the National
Laboratory of the Rockies’ open-source wind turbine models (described in Bodini et al. (in review)) and the coordinates
and dimensions of the King Plains and Armadillo Flats turbines. Participants used these inputs, combined with their own
best practices, to simulate the wind flow around the King Plains and Armadillo Flats wind farms on 24 August 2023.
Phase 1 officially started on 28 May 2024 and participants submitted their simulated data by 1 September 2024.
- 60 – Phase 2: model improvement with inflow observations. The team released all inflow observations and some limited
supervisory control and data acquisition (SCADA) data to participants. Leveraging the additional inflow observations
and insights gained from Phase 1 results, participants tried to improve their simulation results. Phase 2 officially started
on 12 November 2024, coinciding with the release of Phase 1 results. Participants submitted their Phase 2 results by 15
January 2025.
- 65 – Phase 3: model improvement with inflow and wake observations. The team released all inflow and wake observations as
well as all King Plains SCADA data for the selected case study. Participants used this full dataset, along with lessons
learned from the first two phases, to further improve their simulations. Phase 3 officially started on 13 March 2025, with
the release of Phase 2 results. Participants submitted results by 30 April 2025.

Table 1 summarizes the data released to benchmark participants during each phase, while Fig. 1 provides a schematic of the
70 primary observational sites around King Plains (a more comprehensive map is provided in Part 1 (Bodini et al., in review)).

3 Benchmark participants

Universities, research institutes, and private companies (Table 2) from the United States, Denmark, Brazil, Germany, Canada,
France, United Kingdom, Netherlands, and Norway participated in the AWAKEN benchmark. We highlight the main charac-



Table 1. Data released to the benchmark participants in each of the three phases of the exercise.

VARIABLE	SOURCE	SITE	PHASE 1	PHASE 2	PHASE 3	
Wind speed profile upwind	Profiling lidar	A1	✓	✓	✓	
		A2		✓	✓	
		B		✓	✓	
	Scanning lidar	E36			✓	✓
		A1			✓	✓
		A2			✓	✓
		E36		✓	✓	
Wind speed profile downwind	Profiling lidar	C1a			✓	
		H			✓	
	Scanning lidar	H			✓	
		Golf Course			✓	
Temperature profile upwind	Infrared spectrometer	B	✓ (surface only)	✓	✓	
		E36		✓	✓	
Temperature profile downwind	Infrared spectrometer	C1a			✓	
		G			✓	
		Golf Course			✓	
Turbulence profile upwind	Scanning lidar	A1		✓	✓	
		A2		✓	✓	
Turbulence profile downwind	Scanning lidar	H			✓	
Near-surface data upwind	Sonic anemometer	A1	✓ (Obukhov length only)	✓	✓	
		A2		✓	✓	
		A5		✓	✓	
Near-surface data downwind	Sonic anemometer	G			✓	
		H			✓	
Recommended topographical data			✓	✓	✓	
Land use data			✓	✓	✓	
Turbine locations and dimensions			✓	✓	✓	
Cp and Ct curves, RPM, pitch, lift and drag tables	Open-source turbine model		✓	✓	✓	
Curtailment	SCADA	King Plains turbines		✓	✓	
Wind speed (nacelle)	SCADA	King Plains turbines			✓	
Wind direction (nacelle)	SCADA	King Plains turbines			✓	
Power	SCADA	King Plains turbines		✓ (turbines 63–71 only)	✓	
Yaw	SCADA	King Plains turbines			✓	
Yaw misalignment	SCADA	King Plains turbines		✓	✓	

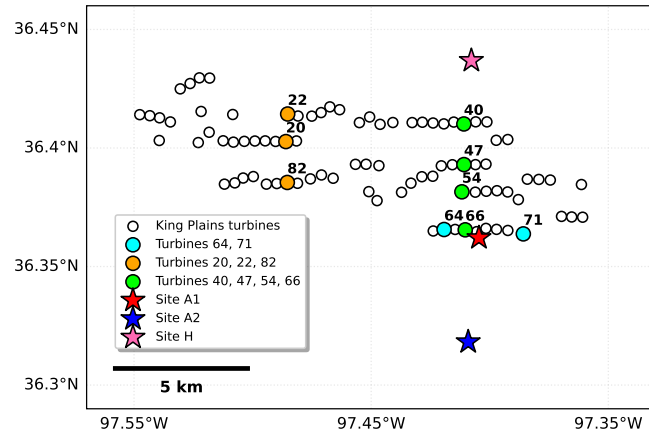


Figure 1. Map showing the King Plains turbines and the locations of sites A1, A2, and H. Highlighted turbines are those selected for detailed analyses in this paper.

85 characteristics of the models used by each participant as well as any changes made in the model setup for those who submitted results in multiple phases of the benchmark. We also note that a few other groups participated in the benchmark but did not give us permission to publish their results.

3.1 Participant 1: PyWAsP by Technical University of Denmark

The wind farm flow was simulated using WAsP, a steady-state model relying on the geostrophic drag law and logarithmic wind profiles (Troen and Petersen, 1989). The wind climate input was derived from lidar observations at 100 m a.g.l. at Site A1 for the 24-hour period from 24 August 2023 00:00 UTC to 25 August 2023 00:00 UTC. The orographic corrections were applied using the model described in Troen and Petersen (1989), and roughness changes were accounted for using the method of Floors et al. (2021). Wake effects were modeled using PyWake’s Park2 offshore model, selected because of its reduced wake decay under nighttime conditions. In phases 1 and 2, the power was corrected by multiplying the power by the modeled local air density and dividing by the one from the power curve (1.225 kg m^{-3}). In Phase 3, power was corrected by using local AWAKEN measurements of air density at Site A1. Stability corrections to the geostrophic drag law were based on a stability model described in Floors et al. (2023) using boundary layer height and heat flux estimates from the National Oceanic and Atmospheric Administration’s High-Resolution Rapid Refresh (HRRR)-Zarr product (Dowell et al., 2022). Both stability and air density were calculated from conditions where the wind speed exceeded the mean wind speed of the whole day, to account for the fact that these conditions are most important for extrapolation of U^3 . The worldcover land cover data (<https://esa-worldcover.org/>) were used, where the mesoscale roughness length for the area is about 0.06 m.

In Phase 2, additional corrections were applied to terrain elevation, and the wind climate was expanded to include lidars from sites A1 and A2. The modelled turbine power output using A1 and A2 as input are then averaged to get an ensemble mean power. A curtailment factor was applied by multiplying with the fraction of time where the turbines were in normal operation.



Table 2. Participants and submission status by benchmark phase.

ID	Participant	Model	Phase 1 submitted?	Phase 2 submitted?	Phase 3 submitted?
1	<i>Technical University of Denmark (DTU):</i> Rogier Floors	PyWAsP	Yes	Yes	Yes
2	<i>Technical University of Denmark:</i> Julian Quick	PyWake + Super Gaussian	Yes		
3	<i>Equinor:</i> Camille Dubreuil, Knut S. Seim	PyWake + Park2/Fuga	Yes x2		
4	<i>Fraunhofer IWES:</i> Jonas Schulte	FOXES	Yes x4		
5	<i>Technical University of Munich (TUM):</i> Desirae Major, Carlo Bottasso	FLORIS	Yes	Yes	Yes
6	<i>Technical University of Denmark:</i> Paul van der Laan	PyWakeEllipSys (RANS)	Yes	Yes	Yes
7	<i>Meteodyn:</i> Ru LI	Meteodyn WT TM (RANS+Park1)	Yes	Yes	Yes x2
8	<i>Equinor:</i> Anh Kiet Nguyen	Weather Research and Forecasting (WRF) + explicit wind farm parameterization (WFP)	Yes	Yes	Yes
9	<i>Pacific Northwest National Laboratory (PNNL):</i> Raj Rai, Colleen Kaul	WRF + Fitch WFP	Yes	Yes	Yes
10	<i>TNO:</i> Kisorthman Vimalakanthan	WRF + Fitch WFP	Yes	Yes	
11	<i>University of Delaware (UDEL):</i> Ali Khanjari, Cristina Archer	WRF + MAV WFP		Yes	
12	<i>University of São Paulo (USP):</i> William Radünz, Bruno Carmo, Luan Parada, David Ricate	WRF + Fitch WFP	Yes x3	Yes	Yes
13	<i>Veer Renewables:</i> Mike Optis	WRF + Fitch WFP	Yes		
14	<i>Technical University of Denmark:</i> Oscar Garcia-Santiago, Alfredo Peña	WRF + Fitch WFP + LES	Yes		
15	<i>Lawrence Livermore National Laboratory (LLNL) and the University of California, Berkeley:</i> Adam Wise	WRF + LES	Yes		Yes
16	<i>Sandia National Laboratories (SNL):</i> Lawrence Cheung, Thomas Herges, Chris Kelley	AMR Wind (LES)	Yes	Yes	Yes



In Phase 3, an indexing error was resolved and the air density was updated using site-specific measurements from AWAKEN.

95 The available power outputs were not used directly for any corrections.

3.2 Participant 2: PyWake + Super Gaussian by Technical University of Denmark

Simulations were performed using the Super Gaussian model (Blondel and Cathelain, 2020) implemented in PyWake (Pedersen et al., 2023). Linear superposition was applied with center-rotor averaging and the 2020 self-similarity blockage model (Troldborg and Meyer Forsting, 2017). The simulation was performed using the WInd Farm API (WIFA) and the exact setup
100 used in the submitted prediction was archived on Zenodo in the WIFA 0.1.0 release under `examples/cases/AWAKEN/wind_energy_system` (Quick et al., 2025) and it is described in detail in Schøler et al. (2026). Data were submitted as 10-minute averages.

3.3 Participant 3: PyWake by Equinor

Two submissions were made using the PyWake model, each employing different engineering wake models: Park2 and PyFuga.
105 The temporal resolution was set to 30-minute averages. For Park2, wake expansion parameters were set with $k = 0.1$ for unstable conditions and $k = 0.061$ for stable conditions. For PyFuga, the parameters were set as $z_i = 1000$ m and $z_0 = 0.001$ m for unstable conditions, and $z_i = 200$ m and $z_0 = 0.001$ m for stable conditions. The input wind speed and direction were taken from the A1 profiling lidar at 80 m a.g.l., with a spatial correction applied to the flow field based on Equinor's WRF data (Participant 8).

110 3.4 Participant 4: FOXES by Fraunhofer IWES

Four submissions using the FOXES model were completed. FOXES is a terrain-following engineering wake model with height-dependent but horizontally uniform inflow. The domain extension is infinite (gridless), and there is no 3D grid resolution because the model is gridless.

The first and second submissions are named FOXES-B14Base and FOXES-B16Base. For both, the temporal resolution was
115 set to 10-minute averages, and the inflow data were directly taken from given measurements, with air density computed using the Boussinesq approximation. The turbulence intensity (TI) was calculated using the given spatially uniform value along with a TI wake model, and background averaging was done using nine weighted vertical points. Both submissions assumed unidirectional wakes, and the power curve results were corrected for air density. In FOXES-B14Base, wake effect averaging used a six-point stepwise two-circle overlap integration, and the wind deficit model followed Bastankhah and Porté-Agel (2014)
120 with linear superposition and a value of $k = 0.1$. The TI wake model used was the Crespo and Hernández (1996) model with quadratic superposition and $k = 0.1$. In FOXES-B16Base, wake effect averaging used a weighted 9x9 grid. The wind deficit model followed Bastankhah and Porté-Agel (2016) with linear superposition, where $k = 0.4$ times the background TI. The TI wake model used was the Frandsen model (Frandsen, 2007).



The third submission is named FOXES-B16D2d5TL. In this case, the wakes propagate with a 2.5-minute time step, following streamline steps based on measurement data that was interpolated to 2.5-minute intervals from 10-minute input data. Additionally, the background information was propagated in a similar manner, assuming that the measurement point represents a whole plane orthogonal to the measured wind vector at each time step. The temporal resolution of the submitted data was 2.5-minute dynamics. The inflow data was taken from the 10-minute measurements, which were then linearly interpolated to 2.5 minutes. All other settings were the same as in the FOXES-B16Base submission.

The fourth and final submission is named FOXES-B16D10. This setup was the same as the third submission, except that here the wakes propagated with a 10-minute time step, with the inflow data directly taken from the given measurements. The temporal resolution of the submitted data was 10-minute dynamics.

3.5 Participant 5: FLORIS by Technical University of Munich

Modeling was conducted using FLORIS (NREL, 2024), and results were submitted as 10-minute averages in Phases 1 and 2 and 1-minute averages in Phase 3. The selected FLORIS models for all simulations include the Gaussian wake model (Bastankhah and Porté-Agel, 2016) and the Crespo-Hernandez wake-added turbulence model (Crespo and Hernández, 1996). In Phase 1, the default parameters of all models were used. In Phase 2, the partial SCADA data was used to calibrate the wake model parameters using the wind farm as a sensor approach (Braunbehrens et al., 2023). In Phase 3, with the availability of all turbine SCADA data, the values for a 9x4 grid of heterogeneous speed nodes was identified using the wind farm as a sensor method to capture inter-/intra-farm and terrain effects on turbine power production that is not accounted for in baseline FLORIS. Heterogeneous speed nodes were determined for wind directions from 120 - 250 degrees (the range of wind directions over the benchmark day) in five-degree increments and for two different times of the day, one set from 0 - 14 UTC and a second set for 14 - 24 UTC to capture the effects of atmospheric stability during the diurnal cycle.

Inflow parameters for the FLORIS simulation at each timestamp of interest on the benchmark day were determined using a combination of the provided scanning and profiling lidar information at location A1. From the profiling lidar, the shear exponent at each timestamp is calculated using the velocity information at different heights and fitting a power law to the profile. From the scanning lidar, the freestream wind speed, wind direction, and turbulence intensity are determined by interpolating the provided data to the turbine hub height. The final inputs to FLORIS power calculations at each timestamp are the velocity, wind speed, turbulence intensity, and shear exponent from the A1 lidar information and the database of heterogeneous speed nodes determined from the wind farm as a sensor tuning.

3.6 Participant 6: PyWakeEllipSys by Technical University of Denmark

Wake simulations were performed using steady-state EllipSys3D-RANS (Michelsen, 1992; Sørensen, 1995) with actuator disks within the PyWakeEllipSys framework (DTU Wind and Energy Systems, 2025). Terrain elevation was included, but a spatially uniform roughness length was assumed. Two time periods were simulated (05:00–07:00 UTC and 17:00–19:00 UTC), representing very stable and unstable atmospheric conditions, respectively. Input wind speed to the model was calculated from the 1 s profiling lidar data from Site A1, aggregated into 2-hour means via intermediate 10-minute bins. The sonic anemometer



data were used to calculate 2-hour Obukhov lengths (L), and zeta ($\zeta = z/L$) values were used to evaluate the applicability of the Monin–Obukhov similarity theory (MOST). However, MOST profiles did not reproduce the observed wind shear accurately. In particular, the stable case had a shallow atmospheric boundary layer (ABL) height (~ 200 m), placing the turbine rotors above the surface layer (for which MOST applies). Thus, MOST was deemed unsuitable for this case, and a simplified ABL inflow model that includes Coriolis forces and parameterized stability was employed (see van der Laan et al. (2024)). The Coriolis parameter is set to match a latitude of 36.33° N ($8.64 \times 10^{-5} \text{ s}^{-1}$). Geostrophic wind speed (9.49 m s^{-1}), roughness length (0.01 m), and a parameter describing the stability of the ABL ($N = 9.57 \times 10^{-3} \text{ s}^{-1}$) were tuned to match observed wind speed and TI at 88.5 m above ground level (a.g.l.). A higher-than-observed ABL height (~ 500 m) was used in the simulations to ensure numerical convergence, at the cost of underestimating shear. An eddy viscosity damping layer was added at $z \sim 400$ m and above to suppress numerical instabilities following (van der Laan et al., 2025).

For the unstable case, an inflow turbulence model based on MOST (Baungaard et al., 2022b) was used with $\zeta = -0.9$, yielding profiles that matched observed shear and TI. The surface roughness (0.223 m) and friction velocity (0.826 m s^{-1}) were derived from MOST theory, following Baungaard et al. (2022a).

In the simulations, the innermost nested domain covered both wind farms using a 12.5 m horizontal resolution. Vertically, 64 and 128 cells were used leading to a total number of 0.555 and 1.28 billion cells, for the unstable and stable cases, respectively. Results of the two steady-state simulations are employed to represent the two 2-hour periods centered at 06:00 and 18:00 UTC. In Phase 2, the turbine layout was updated to correct a minor spatial error. Additionally, air density (ρ) corrections were applied using temporal means derived from the site-specific measurements from AWAKEN. Because the RANS model solution is independent of air density, turbine power P was rescaled during post-processing according to the ratio of the local density:

$$P_{\text{rescaled}} = P_{\text{original}} \frac{\rho_{\text{AWAKEN}}}{\rho_{\text{standard}}} \quad (1)$$

The stable case (05:00–07:00 UTC) initially exhibited significant numerical streaking due to the interaction between the low ABL height and the complex terrain, despite the application of the eddy viscosity damping layer. To mitigate this, in Phase 3 the case was resimulated using a modified ABL inflow method that removes wind veer (van der Laan et al., 2026). No tuning with SCADA measurements from phases 2 and 3 was carried out.

3.7 Participant 7: Meteodyn WT™ by Meteodyn

The wind farm simulations were performed using Meteodyn WT™, a proprietary steady-state RANS model based on a fully coupled multigrid solver (Ferry, 2002). The turbulent-viscosity hypothesis is implemented through a mixing-length model (Pope, 2000). Wake effects were represented using the Jensen Park wake model (Katic et al., 1987). The added turbulence intensity due to wake effects is given by Frandsen model (Frandsen, 2007). The atmospheric boundary layer was modeled using Monin–Obukhov similarity theory. Terrain elevation data were obtained from the United States Geological Survey Digital Elevation Model (10 m resolution) and supplemented with data from the NASA Digital Elevation Model (30 m resolution), while surface roughness conditions were derived from the National Land Cover Database at 30m resolution. The computational domain extends 30 km horizontally with a 50 m spatial resolution, and model outputs were generated at 10-minute instanta-



190 neous intervals. In Phase 1, 24-hour lidar observations at Site A1 were used to prescribe inflow conditions. Measurements of Obukhov length and turbulence characteristics at Site A1 were employed to determine thermal stability within the model. During Phases 2 and 3, the model was further updated to incorporate additional observational data, improving the representation of atmospheric conditions.

3.8 Participant 8: WRF + explicit WFP ensemble by Equinor

195 Simulations utilized WRF version v4.2 with the explicit wake parameterization (WRF-EWP) (Volker et al., 2015). The model was forced with ERA5 data (Hersbach et al., 2020). The horizontal resolution was set to 1000 m, with a vertical resolution stretching from 10 m at the surface to 40 m at 1000 m a.g.l. Output was provided as 10-minute averaged fields derived from 2-minute snapshots. The study adopted an ensemble approach utilizing the Noah land-surface model and varying planetary boundary layer (PBL) and surface-layer (SL) schemes. These included: Mellor–Yamada–Nakanishi–Niino (MYNN) PBL
200 scheme (Nakanishi and Niino, 2009) coupled with the MYNN SL scheme; Mellor–Yamada–Janjic (MYJ) PBL scheme (Mellor and Yamada, 1982) coupled with the MYJ SL scheme; and Yonsei University (YSU) PBL scheme (Hong et al., 2006) coupled with the revised MM5 Monin–Obukhov SL scheme. Turbulence kinetic energy (TKE) advection was enabled for the MYNN and MYJ schemes.

The modeling strategy focused on identifying the best inflow model for each 10-minute time stamp, after which WRF-EWP
205 was used to calculate wake effects without further parameter optimization. Before 18:00 UTC, the "best" model was selected from the full ensemble; after this time, the selection was restricted to the MYNN model to ensure better TKE estimates. The selection criteria evolved across the three phases: Phase 1: The WRF-EWP model utilized a spin-up period of 24 hours to -12 hours relative to 00:00 UTC. The best model was selected based on wind speed and direction data from the A1 profiling lidar. However, because the A1 lidar was located in the same model grid cell as two turbines, the WRF model accounted for wake
210 effects at that location. This resulted in an underestimation of wind speed at A1, which led the selection algorithm to favor models with higher background wind speeds, consequently overestimating power production. Phase 2: This phase utilized the same WRF-EWP models generated in Phase 1, but the selection criteria were refined. The best model was chosen based on power measurements from an averaged turbine (using limited SCADA data released in Phase 2) and a small misfit correction for wind direction at A1. The selection process minimized the totalMisfit at each time stamp:

$$215 \text{ totalMisfit} = \text{scadaMisfit} + \text{windDirMisfit} \cdot 200/30 \quad (2)$$

where *scadaMisfit* is the absolute difference between the mean SCADA power from turbines 63–71 and the mean WRF power for those same turbines. *windDirMisfit* is the absolute difference between the observed wind direction at A1 (100 m a.g.l.) and the WRF 100-m wind direction at that location. Phase 3: New WRF-EWP models were generated using updated turbine layout information to correct a minor layout issue present in previous phases. The spin-up period was reduced to 15 hours, though all
220 other parameters remained identical to Phase 1. The best model was selected using SCADA power measurements from seven front-row turbines on the southern side of the King Plains wind farm (turbines 5, 9, 62, 63, 71, 75, and 88). The misfit was defined as the sum of absolute differences between WRF and SCADA power for these specific turbines.



3.9 Participant 9: WRF + Fitch WFP by Pacific Northwest National Laboratory

225 Simulations used WRF version v4.3 with the Fitch WFP (Fitch et al., 2012), with TKE advection turned on, a TKE coefficient of 25 %. The simulation was performed using a one-way nesting approach. Two nested domains were employed, with horizontal grid spacing of 2904 m and 968 m for the outer and inner domains, respectively. The model was forced with HRRR data (Dowell et al., 2022). The vertical grid spacing up to 400 m a.g.l. was 10 m (reduced to 5 m in Phase 3) and then gradually stretched up to 950 m at the model top. Topography with a resolution of 30 arc-seconds was used in both domains. The model was run with a 12-hour spin-up period before 1-minute instantaneous fields output was saved from the inner domain for the analysis. The model used the MYNN 2.5 PBL scheme (Nakanishi and Niino, 2009) with the MYNN SL scheme, and the Noah land-surface model (changed to Noah-MP in Phase 3). In Phase 2, the turbine layout was updated to correct a minor spatial discrepancy identified in Phase 1.

3.10 Participant 10: WRF + Fitch WFP by TNO

235 Simulations used WRF version v4.3.3 with the Fitch WFP (Fitch et al., 2012), with TKE advection turned off in Phase 1 and on in Phase 2, and a TKE coefficient of 100 %. The model was forced with ERA5 data (Hersbach et al., 2020). The model employed three nested domains, with the innermost domain having a horizontal resolution of 500 m, and varying vertical resolution, with 17 levels in the lowest 200 m. Output was provided as 1-minute instantaneous fields. The model used the MYNN 2.5 PBL scheme (Nakanishi and Niino, 2009) with the MYNN SL scheme, and the Noah land-surface model. In Phase 2, the turbine layout was updated, the spin-up period was extended, and the Fitch parameterization was updated with the Archer et al. (2020) "bug" fix.

3.11 Participant 11: WRF + MAV WFP by University of Delaware

245 Simulations used WRF version v4.3 with the MAV wind farm parameterization (Ma et al., 2022; Khanjari and Archer, 2025), with TKE advection turned on. The model was forced with ERA5 data (Hersbach et al., 2020). The horizontal resolution was 500 m, and vertical resolution was 10 m (in the lowest 300 m). Output was provided as 30-minute averaged fields. The model used the MYNN 2.5 PBL scheme (Nakanishi and Niino, 2009) with the MYNN SL scheme. To represent turbine-induced turbulence, an analytical formulation was developed that replicates the spatial distribution of added TKE observed in LES. The formulation and validation are described in Khanjari et al. (2025). Hub-height wind speed and turbine power were calculated using the XA wake model developed by Ma et al. (2022), using their Superposition Method 3.

3.12 Participant 12: WRF + Fitch WFP by University of São Paulo

250 Simulations used WRF version v4.4 with the Fitch WFP (Fitch et al., 2012), with TKE advection turned on. In Phase 1, three simulations were submitted, corresponding to 0 %, 25 % (Archer et al., 2020), and 100 % added TKE in the wind farm parameterization. In Phases 2 and 3, only the 25 % TKE case was retained. The model was forced with HRRR data (Dowell et al., 2022). The horizontal resolution was 500 m, and vertical resolution was 10 m up to 300 m a.g.l. (and then coarsened



up to a maximum of 500 m). Output was provided as 5-minute instantaneous fields. The model used the MYNN 2.5 PBL
255 scheme (Nakanishi and Niino, 2009) with the MYNN SL scheme, and the Noah land-surface model. In Phase 2, the upstream
domain fetch was shortened compared to Phase 1. In Phase 3, the microphysics scheme was switched from the WRF Single-
Moment 3-class simple ice scheme (WSM3) to the Thompson scheme (Thompson et al., 2008). For this final phase, the team
also considered additional model setups, which were not ultimately selected as they did not better compare with observations.
Three of the tested setups utilized the same 500-m horizontal resolution from phases 1 and 2:

- 260
- A variation of the Phase 2 setup with the land surface model changed to the Rapid Update Cycle (Benjamin et al., 2002);
 - A variation of the Phase 2 setup with the Thompson graupel microphysics scheme;
 - A variation with the Morrison two-moment microphysics scheme (WRF Double-Moment, 7-class, Morrison and Milbrandt, 2011).

An additional four cases utilized a coarser horizontal mesh of 1 km:

- 265
- The Phase 2 setup, but at 1 km horizontal resolution;
 - The Phase 2 setup using the Rapid Update Cycle as the land surface model;
 - A variation with the Thompson microphysics scheme;
 - A variation with the Morrison two-moment scheme.

3.13 Participant 13: WRF + Fitch WFP by Veer Renewables

270 Simulations used WRF version v4.4.1 with the Fitch WFP (Fitch et al., 2012) with the Vollmer modification (Vollmer et al.,
2024), with TKE advection turned on and a TKE coefficient of 100%. The model was forced with ERA5 data (Hersbach et al.,
2020). The horizontal resolution was 500 m, and vertical resolution was 10 m in the lowest 300 m. Output was provided as
10-minute instantaneous fields. The model used the MYNN 2.5 PBL scheme (Nakanishi and Niino, 2009) with the MYNN SL
scheme, and the Noah land-surface model.

275 3.14 Participant 14: WRF-LES + Fitch WFP by Technical University of Denmark

Large-eddy simulations were performed using WRF-LES with actuator disk representations of 32 King Plains turbines in the
innermost domain following the setup of Peña et al. (2022) and Peña and Mirocha (2024). The simulations used five nested
domains, with the innermost grid having a horizontal resolution of 20 m. The model time step was 0.1 s, with output sampled
between 1 s instantaneous and 2-minute averages based on the specific variable. For the mesoscale simulations, WRF version
280 4.2.2 with the Fitch WFP (Fitch et al., 2012), with TKE advection turned on, and 25 % (Archer et al., 2020) added TKE
in the wind farm parameterization. The model was forced with ERA5 reanalysis data (Hersbach et al., 2020). The model
used the MYNN 2.5 PBL scheme (Nakanishi and Niino, 2009) with the MYNN surface-layer scheme, and the Unified Noah
land-surface model.



285 **3.15 Participant 15: WRF-LES by Lawrence Livermore National Laboratory and the University of California, Berkeley**

WRF-LES (base code WRF version 4.4) simulations were conducted with two nested domains in Phase 1 and three nested domains in Phase 3 with all simulations forced using data from the HRRR model v4 (Dowell et al., 2022). For all simulations, the finest domain utilized a generalized actuator disk (Mirocha et al., 2014) to represent 50 individual King Plains wind turbines. The setup in Phase 1 followed the setup from Wise et al. (2025). For both phases, the outermost domain had 300 m horizontal resolution and 1 s temporal resolution and used the TKE-1.5 LES closure scheme (Deardorff, 1980). The innermost domain had 20 m horizontal resolution, and 0.05 s temporal resolution. Here, the dynamic Wong–Lilly subgrid scheme (Wong and Lilly, 1994) was added to the base code and used along with a near-surface canopy parameterization (Brown et al., 2001). A middle domain was added in Phase 3 and was run with 100 m horizontal resolution and 0.25 s temporal resolution, also with the dynamic Wong–Lilly subgrid scheme. All domains had the same vertical grid resolution of about 8.5 m near the surface, with a gradual coarsening higher up. The following physical parameterizations were used across all domains: the Noah land surface model (Chen and Dudhia, 2001), the Rapid Radiative Transfer Model for longwave radiation (Mlawer et al., 1997), the Dudhia shortwave radiation model (Dudhia, 1989), and the Monin–Obukhov (Janjic Eta) surface layer scheme (Janjić, 1994). Due to their computational expense, the simulations were only run during two periods with distinctly different atmospheric conditions. The first period had stable conditions (05:00-07:00 UTC) while the second period had unstable conditions (17:00-19:00 UTC). Additionally, output was provided as 1 s instantaneous data.

310 **3.16 Participant 16: AMR-Wind by Sandia National Laboratories**

LES runs were performed using AMR-Wind (Kuhn et al., 2025). The computational mesh employed adaptive refinement, with a base resolution of 10 m and refined mesh cells of 2.5 m in the rotor region. A one-equation k-sgs subgrid model was used along with the Boussinesq approximation. The simulations excluded terrain and moisture effects. Output was provided as 0.1 s instantaneous data. The simulations targeted three distinct periods. Stable conditions were modeled in Phase 1 (04:55–06:00 UTC) and Phase 3 (05:00–07:00 UTC), while unstable conditions were modeled in Phase 2 (16:45–18:49 UTC). Phase 3 introduced several methodological updates compared to Phase 1: the precursor generation incorporated full observed temperature profiles rather than relying on surface temperature and estimated profiles; the simulation domain was restricted to the King Plains wind farm; and active yaw control was enabled for all turbines.

310 **4 Modeling benchmark results**

In this section, we evaluate the performance of the participating models across the three phases of the benchmark. This progressive analysis allows us to disentangle the sources of error by moving from a blind prediction state (Phase 1) to stages where inflow (Phase 2) and wake (Phase 3) observations were released to allow modelers to improve their model accuracy.



Note that the native model resolution (and whether average or instantaneous data were used) for each submission is applied to
315 the observations when calculating error metrics or making comparisons, unless specified otherwise.

4.1 Phase 1: Baseline performance and physical drivers of error

The Phase 1 analysis begins by evaluating the baseline performance of participating models in predicting total power production
at the King Plains wind farm (Fig. 2). In general, simpler models driven by point measurements of wind speed (provided
at Site A1 in Phase 1) captured the temporal variability of power production more accurately than more complex models.
320 Mesoscale models (and LES coupled to WRF) struggled to reproduce some of the observed variability, particularly under
stable conditions. Notably, most models forced by reanalysis products (ERA5 or HRRR) failed to capture the sharp drop in
wind speed and power production observed around 05:00 UTC. A significant exception was the WRF submission by Equinor,
which successfully reproduced this feature, likely due to an ensemble selection strategy that filtered for the member that best
matched the provided wind speed observations at Site A1.

325 To understand the physical drivers behind the discrepancies observed in the time series, we examine the observed and
modeled vertical structure of the wind flow during a critical time (06:00 UTC) in stable conditions. As detailed in Part 1
(Bodini et al., in review), this period is characterized by a strong low-level jet (LLJ) interacting with the turbine rotor layer,
where jet lifting leads to a drop in power production. Wind speed profiles at Site A1 reveal significant discrepancies between
models and observations during this period (Fig. 3). Because Phase 1 only provided observations of wind speed at Site A1
330 up to 240 m a.g.l., simpler models (e.g., PyWake+SuperGaussian and FOXES) that directly ingested these data matched
the lower profile well but suffered from extrapolation errors aloft. In the absence of upper-level observations, these models
often assumed profile shapes that deviated significantly from the actual LLJ structure. Some other models used monotonically
increasing profiles that did not reflect the observed conditions. Conversely, WRF-based models relying on reanalysis forcing
consistently underestimated the LLJ strength and placed the jet nose at a lower altitude than observed. This general inability to
335 accurately resolve the inflow shear profile under real-world scenarios is a primary driver of the power production errors.

These upstream inflow deficiencies propagated downstream, complicating the resolution of wind speed profiles downwind of
the wind farm, as wake effects and terrain interactions added further complexity to the flow. At Site H, located approximately
22 rotor diameters downwind, observations reveal a complex vertical structure (Fig. 4): a clear wind speed deficit aloft and
flow acceleration near the surface, which is a phenomenon consistent with long-term observations at this site (Bodini et al.,
340 2021). Given that the deficit is most pronounced above hub height, this feature is likely attributable to the terrain- and wind
farm-induced lifting of the LLJ identified in Bodini et al. (in review), rather than wake effects alone. Capturing this deficit
proved difficult for most models. Steady-state and most RANS approaches generally struggled to reproduce the specific nosed-
deficit profile shape characteristic of the LLJ. The PyWakeEllipSys RANS approach was able to maintain the nosed-deficit
profile, though at heights above those observed, possibly because the inflow ABL height was set to a higher value compared to
345 the inflow data to maintain numerical stability, as discussed in Sect. 3.6. WRF-based and LES submissions generally captured
the presence of the nosed deficit but struggled to correctly predict its vertical height and intensity, mirroring their difficulties

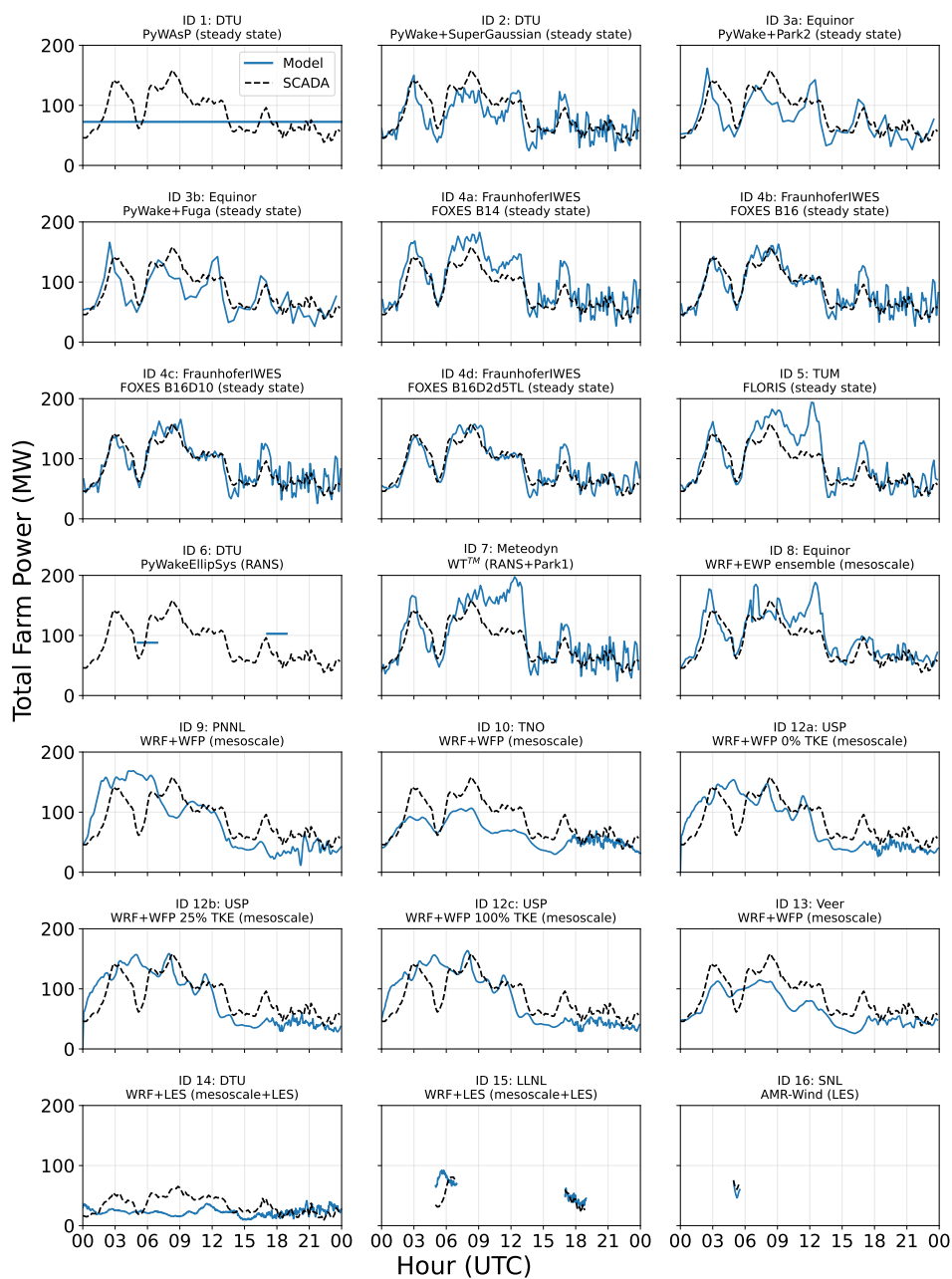


Figure 2. Time series of modeled and observed power at the King Plains wind farm on 24 August 2023 for each Phase 1 benchmark submission. Note that for submissions modeling only a subset of the turbines, the observed and modeled totals are calculated using only the corresponding turbines. Across all submissions, observed data are plotted at 10-minute resolution to increase readability. For the same goal, LES-modeled data are plotted using 2-minute instantaneous values.

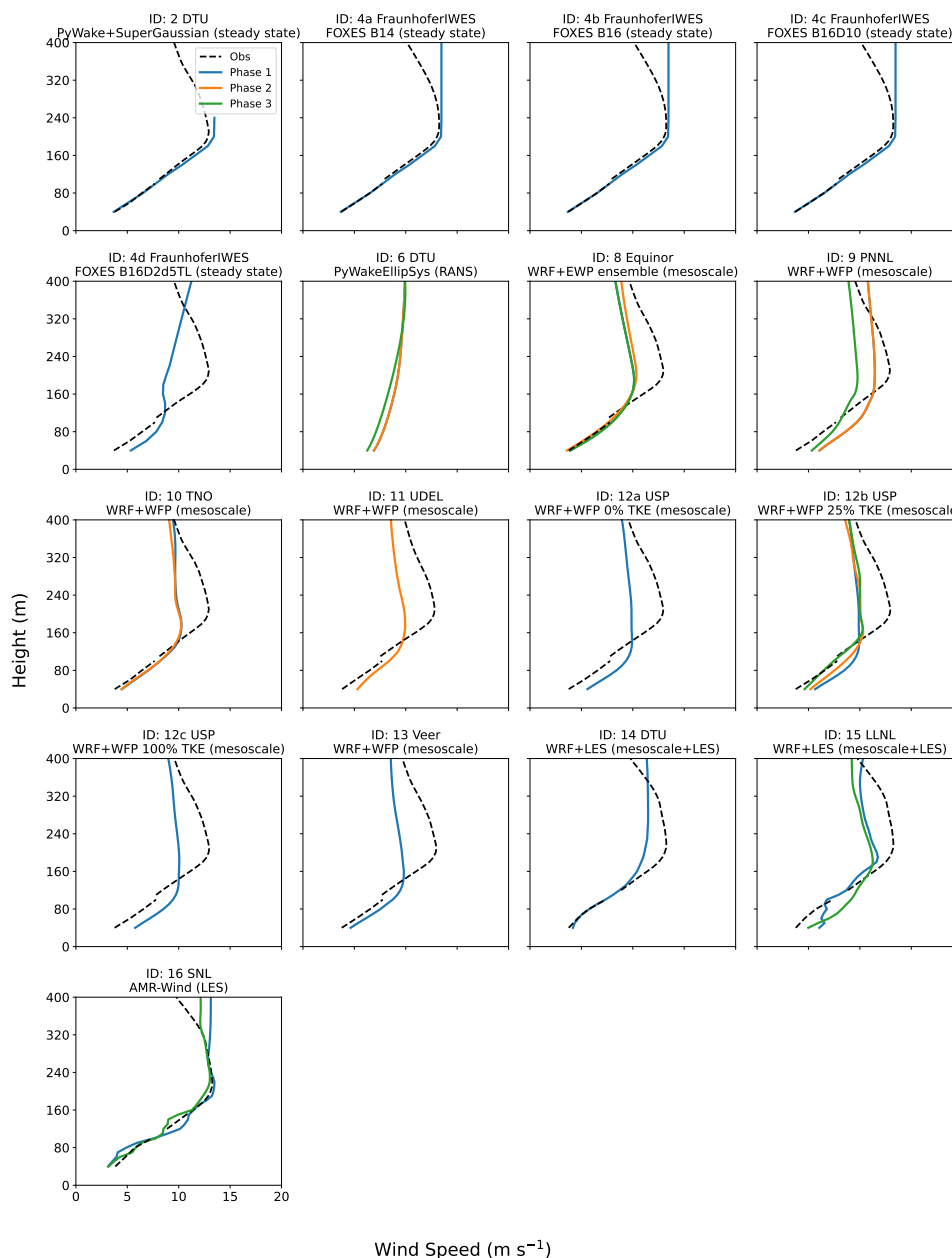


Figure 3. Modeled and observed wind speed profiles at Site A1 at 06:00 UTC on 24 August 2023. Profiles transition from profiling lidar data (≤ 100 m a.g.l.) to scanning lidar measurements (> 100 m a.g.l.); the discrepancy at this interface represents the inherent measurement uncertainty during instrument hand-off. Observations are matched to the time resolution (and average vs. instantaneous) of each model submission. Only models that submitted wind speed information at Site A1 are included in the plot. Meteodyn WTTM results are not included as the model is designed to provide long-term mean wind profile, not instantaneous snapshots.



with the upstream inflow profile. Notably, however, some WRF submissions and all LES-based models were able to capture the flow acceleration closer to the surface.

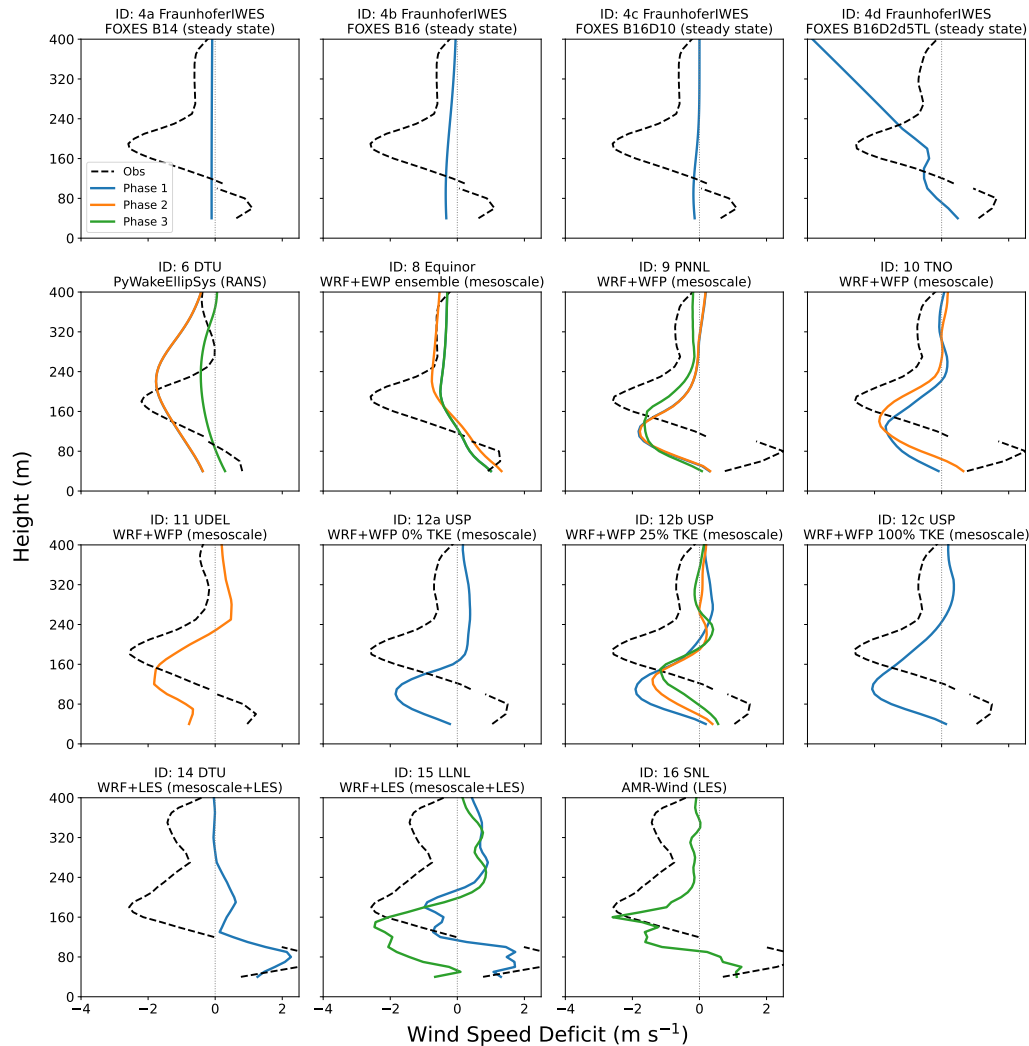


Figure 4. Modeled and observed wind speed deficit profiles, calculated as the difference between wind speed at sites H and A1, at 06:00 UTC on 24 August 2023. Observations are processed to match the time resolution and temporal treatment (averaged versus instantaneous) of each model submission and may therefore appear different across panels. Profiles transition from profiling lidar data (≤ 100 m a.g.l.) to scanning lidar measurements (> 100 m a.g.l.). Only models providing data at both sites are shown. Meteodyn WTTM results are not included as the model is designed to provide long-term mean wind profile, not instantaneous snapshots.

350 Correctly characterizing freestream conditions proved to be a prerequisite for accurate farm modeling. To isolate this "inflow error floor," we examine the power production of turbines 64 and 71 (highlighted in cyan in the map in Fig. 1), which are located in the southernmost (inflow) row and do not experience internal farm wakes under southerly flow. The comparison of



modeled and observed power for these turbines (Fig. 5) reveals a widespread inability to capture the spatial heterogeneity of the inflow. Despite being separated by only ~ 3 km in relatively simple terrain, observations show that turbine 71 (red dashed line) frequently produces more power than turbine 64 (blue dashed line) during stable conditions: between 8:00 and 9:00 UTC
355 turbine 71 output about 1 MW more power than turbine 64. Most mesoscale and LES-based models fail to track these sharp power fluctuations and the observed spatial variability, often overestimating production by more than 1 MW during the LLJ interaction between 04:00 and 06:00 UTC and, more broadly, in stable conditions. While simpler steady-state models driven by point measurements can follow the general trend of the observations, they often fail to differentiate between the two turbines, predicting nearly identical power for both. This spatial heterogeneity in the observed inflow—and the models' general inability
360 to reproduce it—suggests that a substantial portion of the total benchmark error is inherited from the inflow specification rather than wake physics alone.

Expanding the analysis to the full array reveals substantial inter-model variability in power bias across the wind farm (Fig. 6). Model complexity was not a primary predictor of accuracy; high-fidelity models, such as LES or mesoscale-coupled approaches, did not uniformly outperform simpler engineering or steady-state models in terms of bias. Variability is evident not
365 only across different modeling approaches but also within the same family of models (e.g., the various WRF submissions), highlighting the high sensitivity of results to user-defined configurations such as the reanalysis product, PBL scheme, or grid resolution. Furthermore, a systematic spatial trend is observable across the majority of submissions: turbines in the southwestern region generally exhibit positive (or less negative) biases, while turbines in the northeastern sector show distinct negative (or less positive) biases. This southwest-northeast gradient suggests a widespread difficulty in capturing the spatial heterogeneity of the flow field across the site, likely driven by the complex terrain-flow interactions described in the Part 1 paper (Bodini et al., in review) and in Radünz et al. (2025).
370

Because bias metrics can mask performance issues through error compensation, we also examine the mean absolute error (MAE) in turbine-level power production (Fig. 7). Consistent with the bias results, significant variability exists across model types. The spatial analysis reveals that waked turbines generally exhibit higher MAE values compared to freestream turbines,
375 reflecting the added complexity of accurately resolving wake deficits and recovery compounded by terrain-induced acceleration effects.

The spatial patterns in bias and MAE point to a strong topographic influence on model performance. As noted in the Part 1 analysis (Bodini et al., in review) and in Radünz et al. (2025), observational data revealed a counterintuitive phenomenon where turbines in the waked rows of the King Plains wind farm produced higher power output, attributed to terrain-induced
380 flow acceleration. To quantify this topographic influence, we define a relative elevation metric Δz_{rel} for each turbine as:

$$\Delta z_{rel} = z_{turbine} - \bar{z}_{upstream} \quad (3)$$

where $z_{turbine}$ is the actual physical base elevation of the turbine and $\bar{z}_{upstream}$ is the mean physical terrain elevation within a 1 km upstream sector (defined by a 45° arc centered on the mean hub-height wind direction). A negative Δz_{rel} indicates the turbine is situated in a local depression or at the base of a downward slope relative to the upwind terrain, while a positive value indicates a local topographic high, such as a ridge. Plotting turbine-level MAE against Δz_{rel} reveals a prevalent
385

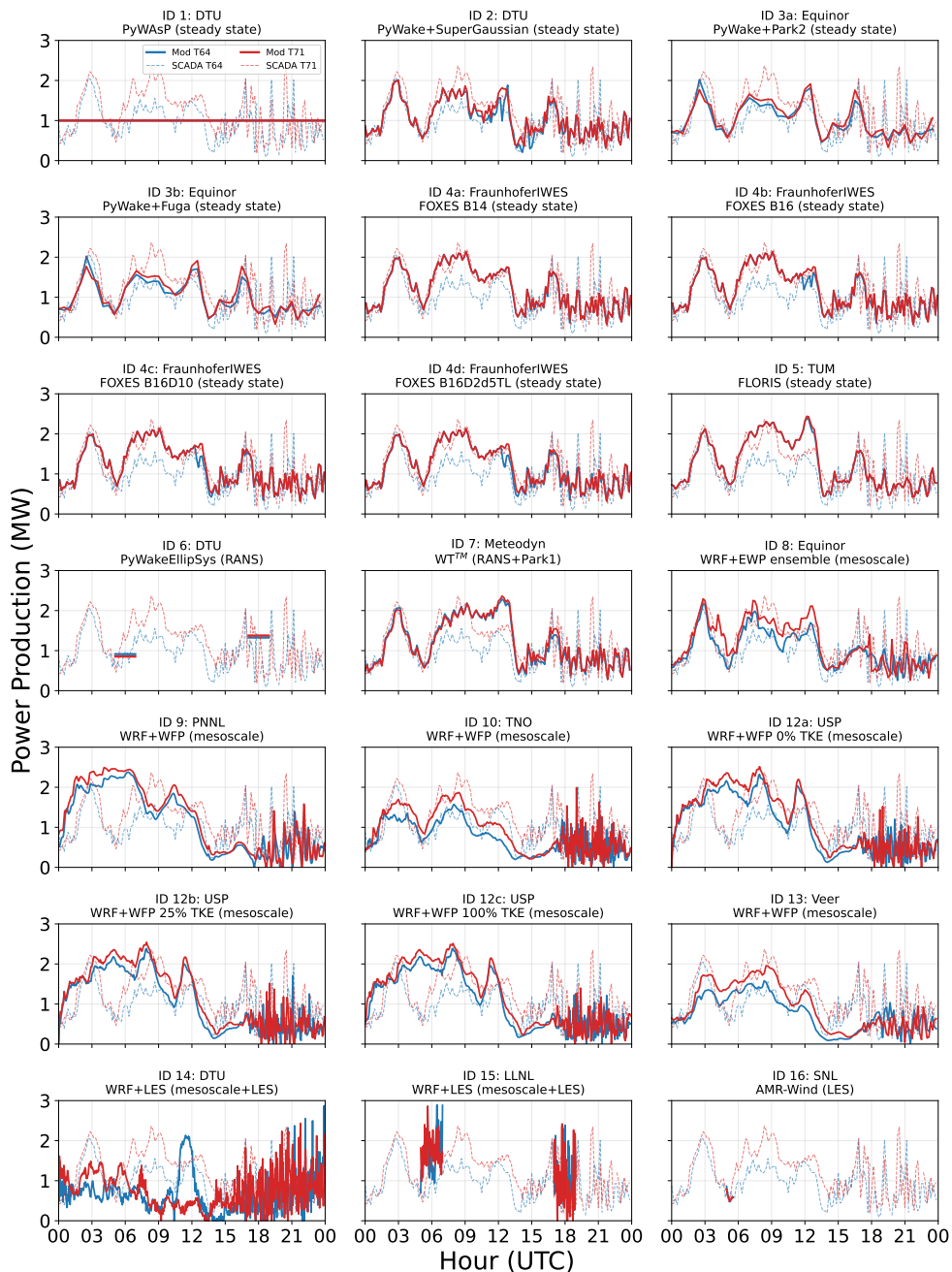


Figure 5. Time series of modeled and observed power at two selected inflow turbines (IDs 64 and 71, see map in the Part 1 paper) within the King Plains wind farm on 24 August 2023 for each Phase 1 benchmark submission. Across all submissions, observed data are plotted at 10-minute resolution to increase readability. For the same goal, LES-modeled data are plotted using 2-minute instantaneous values.

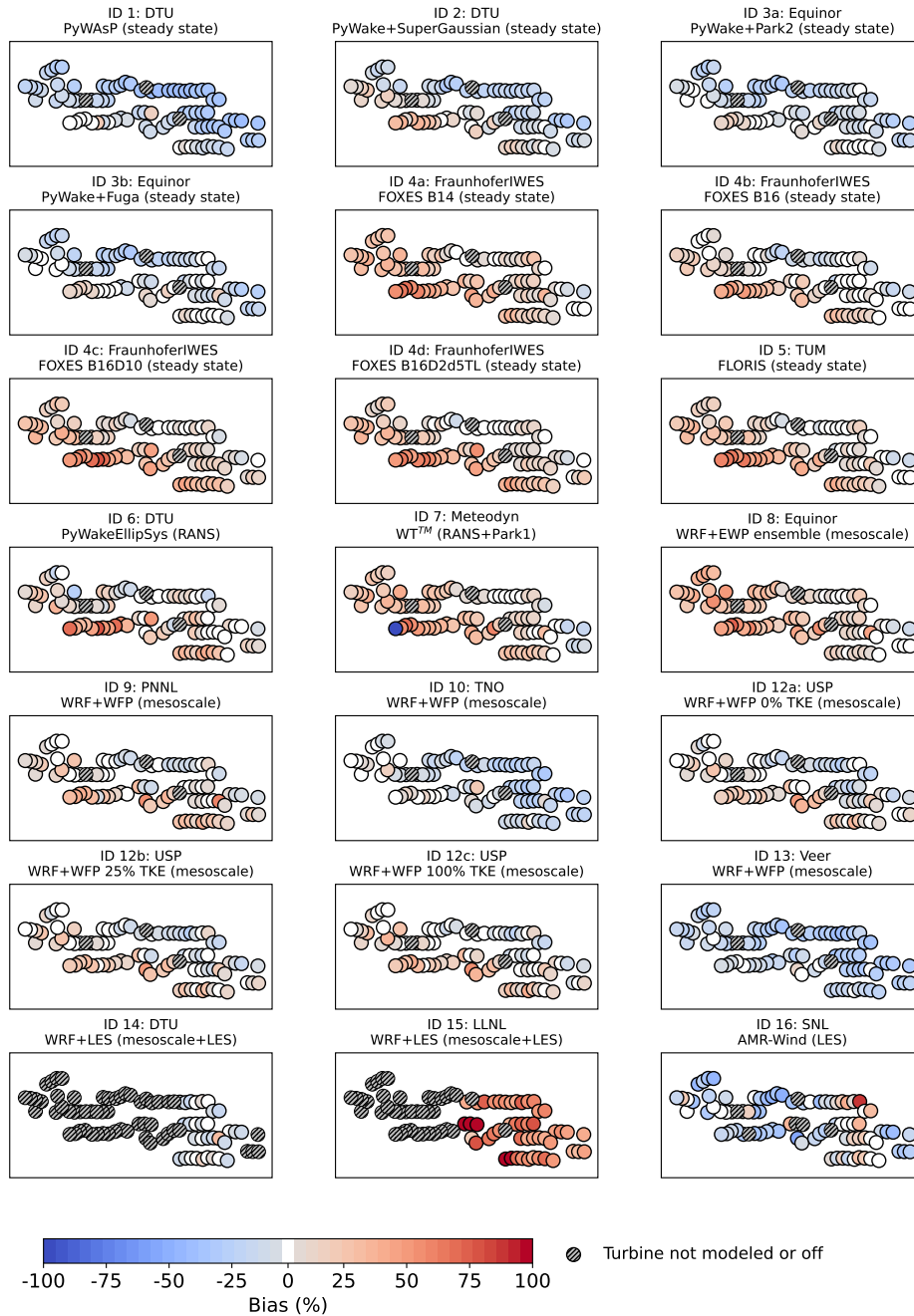


Figure 6. Maps showing the percentage bias in modeled vs. observed power produced by each turbine in the King Plains wind farm on 24 August 2023 for each model submission to Phase 1 of the benchmark.

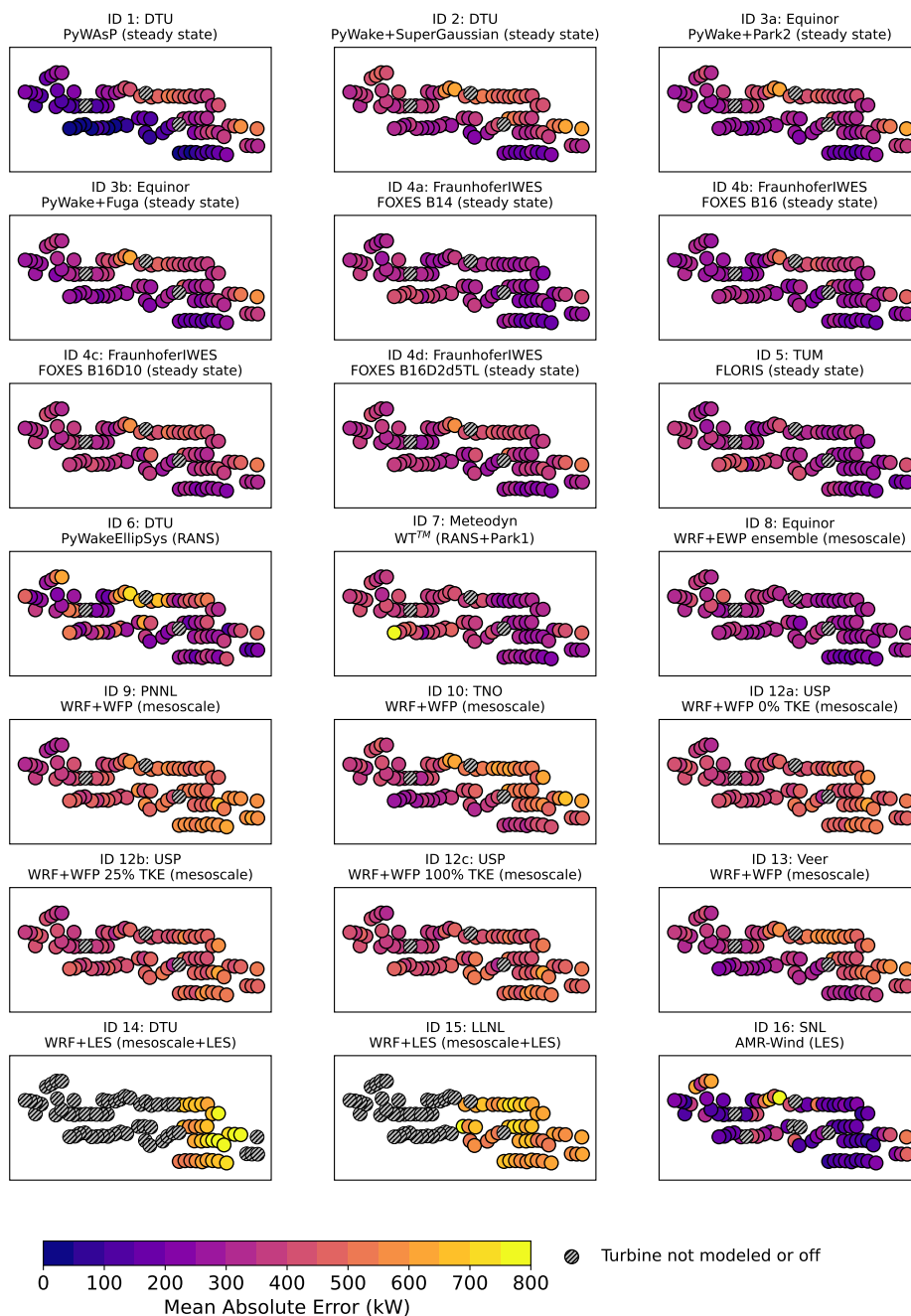


Figure 7. Maps showing the mean absolute error in modeled vs. observed power produced by each turbine in the King Plains wind farm on 24 August 2023 for each model submission to Phase 1 of the benchmark.



negative correlation across the majority of submissions (Fig. 8). This indicates that models exhibit higher errors at turbines situated at elevations lower than the upstream terrain, confirming the difficulty in capturing the interaction between wakes and terrain-induced speed-ups. This negative correlation is generally stronger for stable conditions (Fig. S1 in the Supplementary Information) while most models show weaker correlations (sometime even positive) during turbulent, unstable conditions (Fig. 390 S2). While most engineering models generally show strong negative correlations, results for higher-fidelity approaches are mixed. The FLORIS submission shows a weak positive correlation in Phase 1, deviating from the general trend. However, as shown in the Supplementary Information (Figs. S3 and S4), this correlation shifts to negative in subsequent benchmark phases, suggesting that as inflow errors are corrected via model calibration, the underlying terrain-induced physics becomes the dominant remaining source of spatial error.

395 The significant impact of local topography reinforces the observation made earlier in this section: substantial prediction errors persist even for turbines unaffected by upstream wakes. To weigh the relative contributions of these baseline errors (driven by terrain and inflow specification) versus wake physics to the total error, we compare the aggregate MAE for inflow and waked turbines (Fig. 9). Across all Phase 1 submissions, the mean MAE for inflow turbines exceeded 300 kW (~11 % of the nameplate capacity), while the mean MAE for waked turbines averaged over 400 kW (~14 % of the nameplate capacity). 400 This comparison indicates that difficulties in accurately representing inflow conditions contribute significantly to the total error, suggesting that wake modeling inaccuracies are not the sole, or perhaps even the primary, driver of performance losses in real-world complex terrain. Interestingly, a subset of the WRF-based models exhibits near-equal or even lower error for waked turbines than for inflow turbines. This result reinforces the conclusion that for mesoscale approaches, prioritizing improvements in inflow representation—potentially through better ensemble selection or data assimilation—may yield larger accuracy gains 405 than focusing on wake parameterization alone. Finally, the data highlight substantial variability in model results between neighboring wind turbines; these localized discrepancies point to microscale terrain features or complex wake interactions that remain difficult to capture consistently.

Segregating performance by atmospheric stability (using the Obukhov length calculated from sonic anemometer measurements at Site A1) further highlights the physical challenges faced by the models (Fig. 10). Generally, models exhibited higher 410 MAE under stable conditions, consistent with the difficulties of resolving shallow mixing depths, strong shear and terrain-induced accelerations in the stable boundary layer. While the farm-averaged bias metric displays no clear systematic trend across all models favoring one stability class, the results reveal a critical trade-off between systematic bias and absolute error in time-resolved modeling. Notably, the DTU WRF+LES submission achieves a near-zero bias for the complete period (driven by a compensating effect between a large negative bias in stable conditions and a large positive bias in unstable conditions) yet 415 exhibits the highest MAE of all participants. This discrepancy, shared by other high-fidelity submissions, illustrates the “double penalty” effect inherent to simulations resolved at fine time resolution: unavoidable phase errors in simulating high-frequency wind fluctuations increase the absolute error, whereas steady-state models that target the mean flow circumvent these timing penalties, often resulting in lower MAE despite potentially larger systematic biases.

Finally, to isolate the internal physics of wake propagation from inflow errors, we computed correlations between observed 420 and modeled power ratios for selected turbine pairs (Fig. 11). For this analysis, each ratio is defined with a waked turbine in the

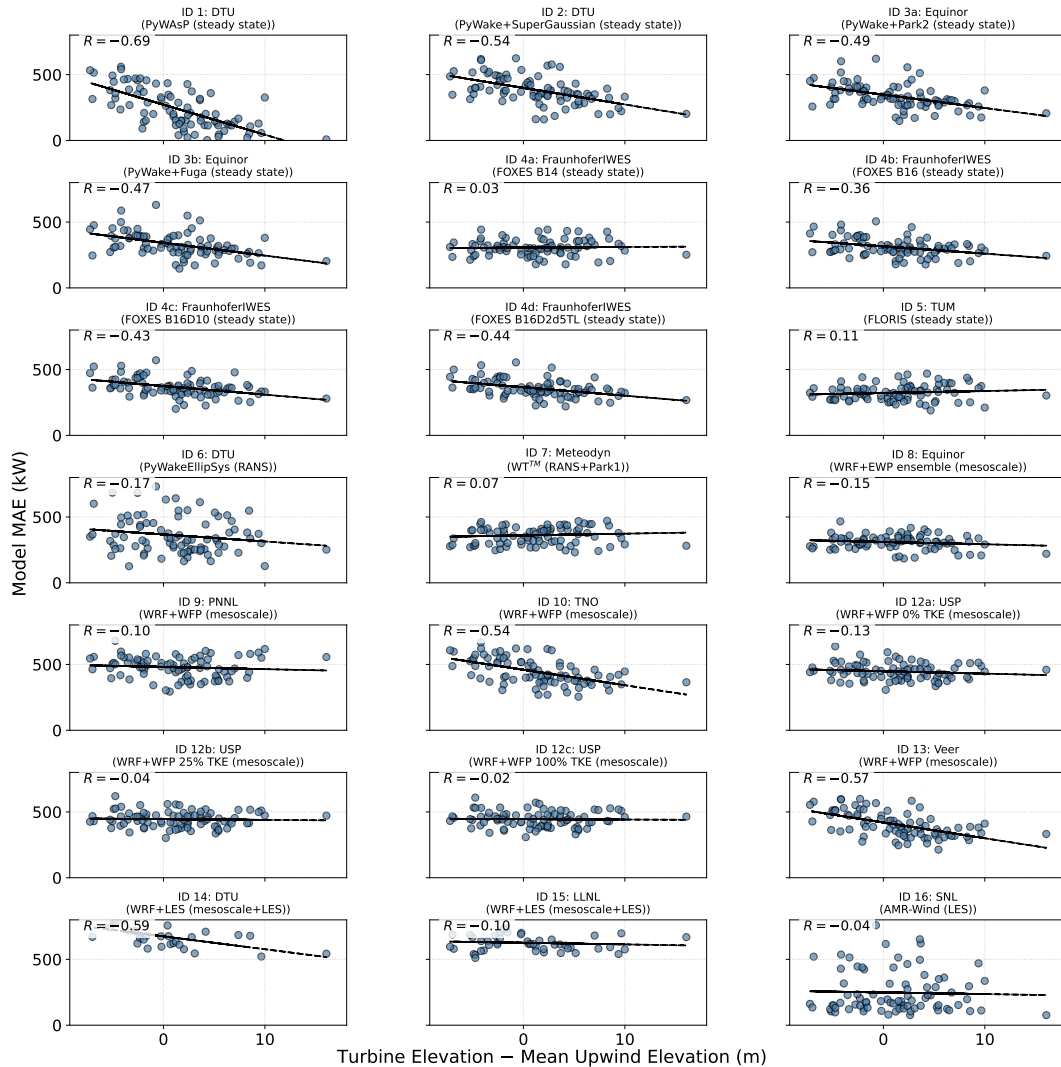


Figure 8. Scatterplots of turbine-level MAE vs. relative terrain elevation for each Phase 1 model submission.

numerator and an upwind turbine (located in the southernmost row) in the denominator. The selected turbines are highlighted in orange (western transect) and green (eastern transect) in the map in Fig. 1. Overall, the resulting correlations are relatively low, indicating that capturing the specific temporal dynamics of wake losses remains a challenge for most modeling approaches. However, under stable conditions (Fig. 12) – which are characterized by less chaotic flow and reduced turbulence – correlations increase across the board, even though the MAE is generally higher in these regimes. This distinction underscores that while errors in inflow and terrain representation dominate the absolute power prediction, the relative wake dynamics are better resolved during stable stratification, likely because the reduced ambient turbulence leads to more persistent wake structures that are less obscured by meandering and mixing. In contrast, the lower correlations observed in unstable conditions (Fig. S5

425

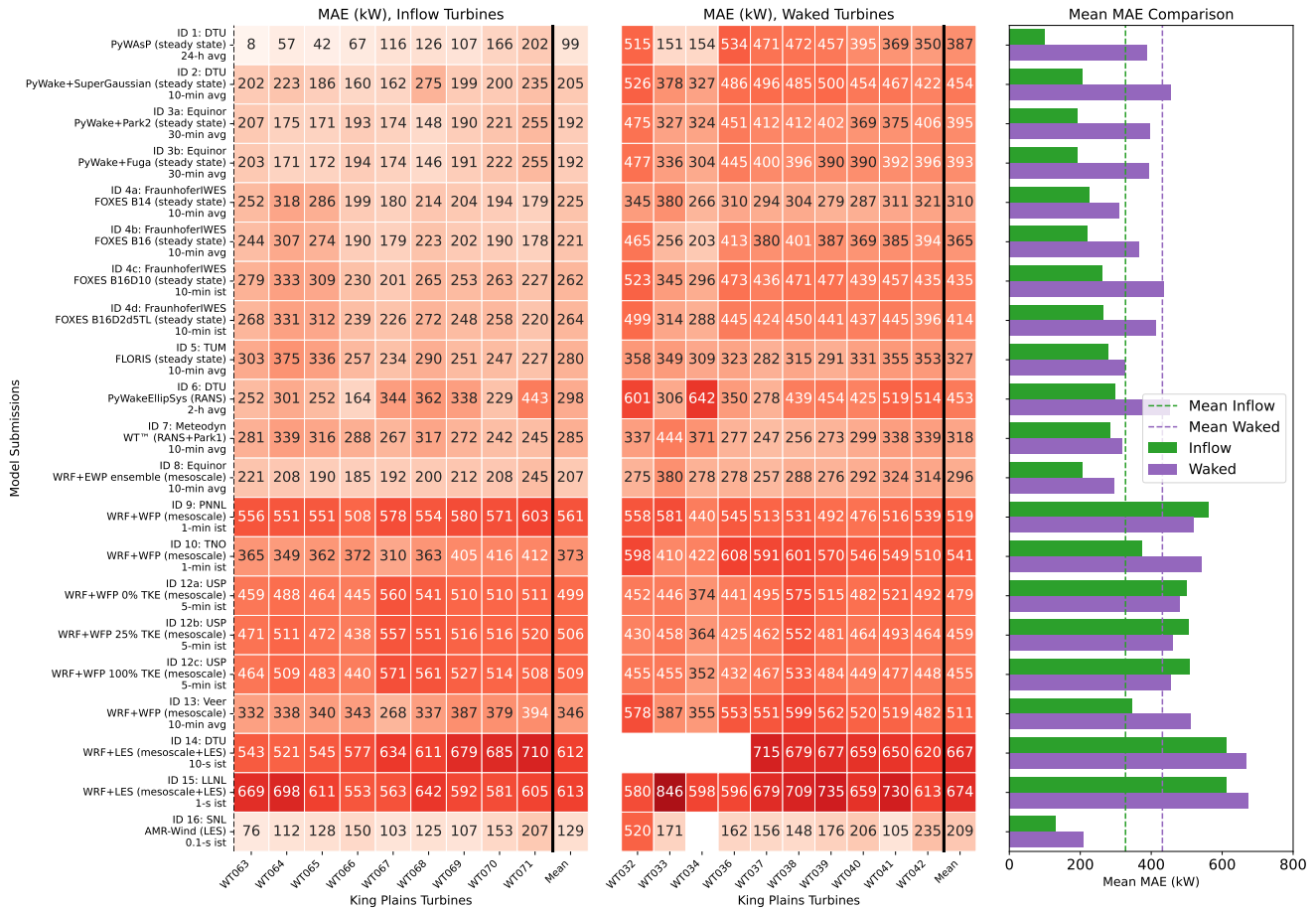


Figure 9. MAE in modeled power for selected turbines in the southern (inflow) row of King Plains (left) and the northern (waked) row (middle). The bar chart on the right compares the mean MAE across all submissions for inflow vs. waked turbines. Results for Phase 1.

in the Supplementary Information) reflect the inherent difficulty of tracking high-frequency turbulent fluctuations in the time domain. Spatially, most models consistently exhibit higher correlations for specific turbine pairs, such as those associated with Turbine 20 (second row, western sector) and Turbine 47 (third row, eastern sector). Notably, we observe no systematic reduction in correlation strength in the western portion of the farm, suggesting that the external farm-to-farm wakes from Armadillo Flats did not significantly degrade the models’ ability to capture relative wake dynamics compared to the eastern section.

4.2 Evolution of model errors through phases 2 and 3

In phases 2 and 3, modelers were provided with progressively richer observational datasets, culminating in the release of SCADA data for all King Plains turbines for the benchmark day in Phase 3. The modeled wind speed profiles at Site A1 (Fig. 3) exhibited only limited variations in phases 2 and 3 compared to the baseline, reflecting the constraints many models face

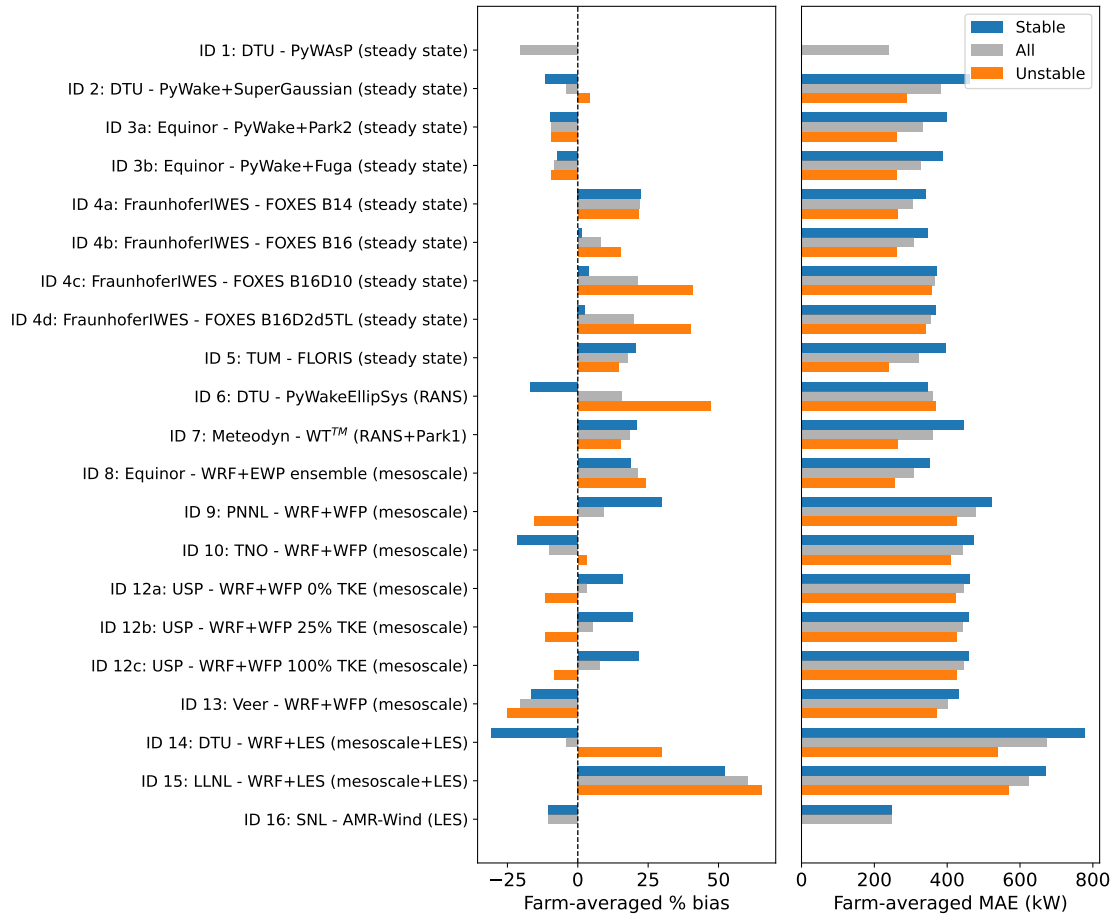


Figure 10. Histograms showing the farm-averaged percentage bias (left) and MAE (right) in modeled vs. observed power produced by the King Plains wind farm on 24 August 2023 for each model submission to Phase 1 of the benchmark.

in directly assimilating single-point profile observations. However, more distinct variations are evident in the modeled wind speed deficit profiles (Fig. 4), suggesting that updates to model setups, such as calibration or refined boundary conditions, had a more pronounced impact on the representation of wake recovery.

The impact of this additional data access on model performance is first examined through the time series of farm-level power production shown in Figs. 13 and 14. Phase 2 results show a general improvement over the baseline (Fig. 13). Access to detailed inflow atmospheric data and SCADA from inflow turbines allowed participants to refine their boundary conditions and internal parameters. For instance, the FLORIS simulation showed improved agreement with observations, effectively filtering out the unrealistic peaks observed in Phase 1. However, challenges persisted for mesoscale models, which continued to struggle with the sharp power drop associated with the LLJ lifting at 05:00 UTC. In Phase 3, the release of full SCADA data enabled direct model calibration, leading to significant performance gains (Fig. 14). The FLORIS model, now tuned to the provided power



Figure 11. Pearson correlation coefficients between observed and modeled power ratios for selected turbine pairs during Phase 1. The ratios are calculated as the power of the waked turbine divided by the power of a corresponding upstream reference turbine in the southernmost row, for turbines in the western (left) and eastern (right) portions of King Plains.

data, achieved a remarkable match with observations. Physics-based models also demonstrated marked improvements; the

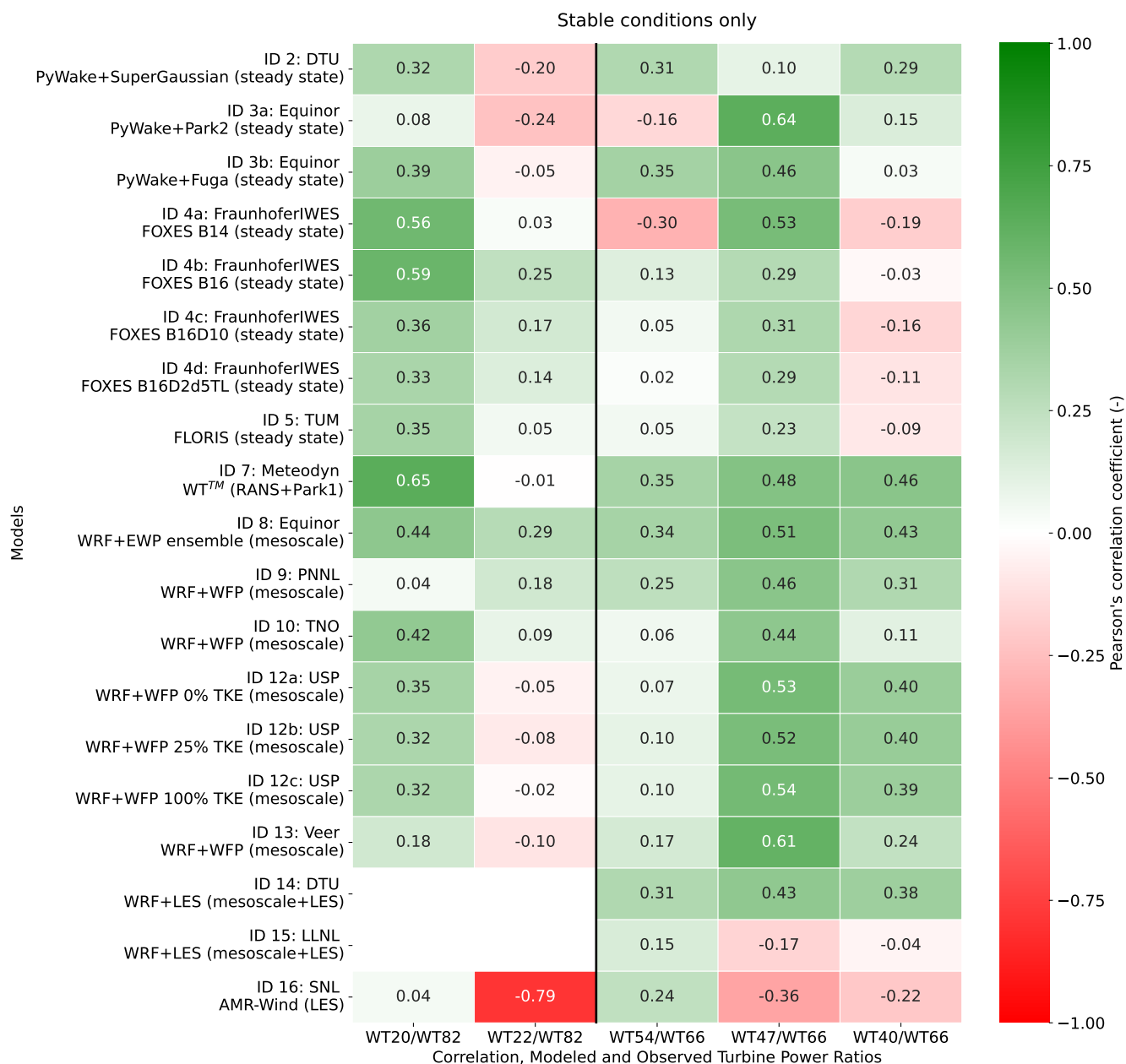


Figure 12. Pearson correlation coefficients between observed and modeled power ratios between turbine pairs during Phase 1, calculated using only data from stable atmospheric conditions, for turbines in the western (left) and eastern (right) portions of King Plains.

RANS submission by Meteodyn, the WRF submission by Equinor, and the steady-state PyWAsP model by DTU all achieved 450 high accuracy. The Sandia LES model also performed well.

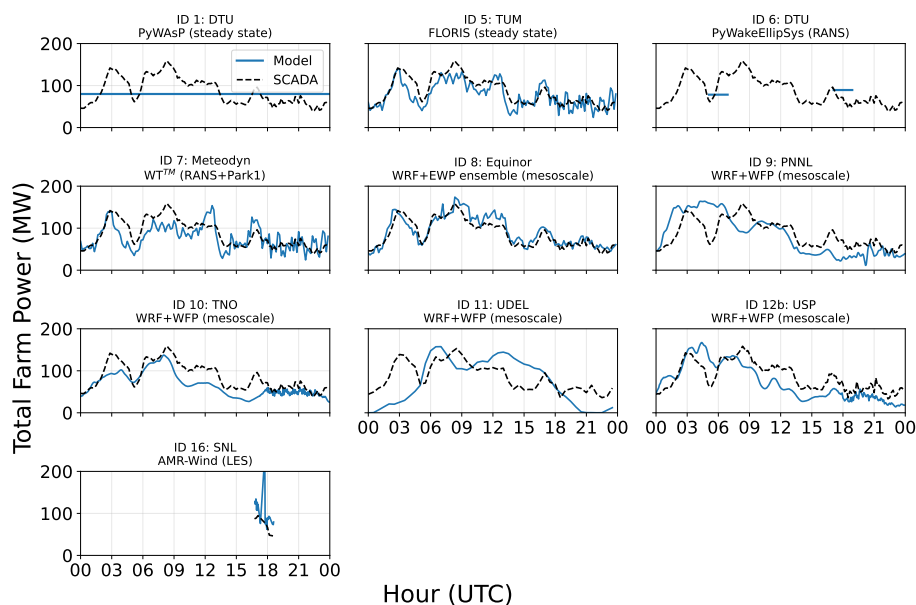


Figure 13. Time series of modeled and observed power at the King Plains wind farm on 24 August 2023 for each Phase 2 benchmark submission. Note that for submissions modeling only a subset of the turbines, the observed and modeled totals are calculated using only the corresponding turbines. Across all submissions, observed data are plotted at 10-minute resolution to increase readability. For the same goal, LES-modeled data are plotted using 2-minute instantaneous values.

While spatial variability persists, specific models demonstrated marked improvements in bias reduction as participants leveraged the additional data (Figs. 15 and 16). For example, the availability of detailed inflow profiles allowed for corrections in background flow fields that mitigated some of the spatial gradients observed in Phase 1, particularly for models capable of directly assimilating observational data rather than relying solely on reanalysis forcing. It is important to note that the Sandia submission (AMR-Wind) modeled a different temporal window in Phase 2 (unstable conditions) compared to Phase 1 (stable conditions), resulting in a distinct error distribution for that specific submission.

The evolution of MAE through phases 2 and 3 confirms that the majority of models achieved a reduction in error (Figs. 17 and 18). However, a persistent spatial pattern remained for most participants, characterized by larger MAE values in the waked portion of the wind farm compared to the inflow row. When looking at MAE values for selected inflow and waked turbines in the eastern (unwaked by Armadillo Flats) portion of the King Plains wind farm (Figs. S6 and S7 in the Supplementary Information), the error in modeled power for the inflow turbines still accounts for about two-thirds of the error seen for the waked turbines, on average. A notable exception was observed in the University of Delaware's submission (WRF with a customized WFP); in Phase 2, this model successfully mitigated the high bias previously observed in the northeastern portion of the farm, likely due to a refined calibration of the TKE parameterization. As already noted in Phase 1, most models had larger

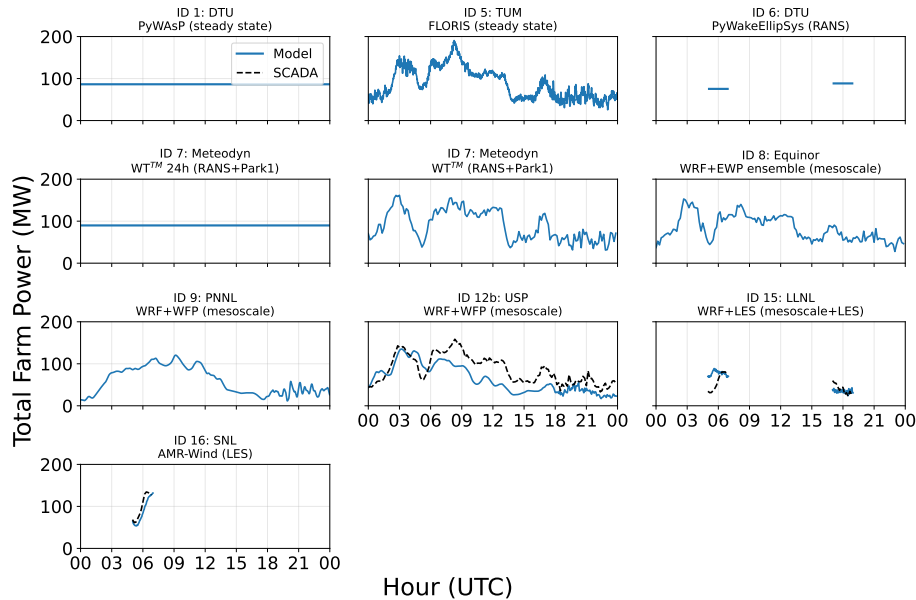


Figure 14. Time series of modeled and observed power at the King Plains wind farm on 24 August 2023 for each Phase 3 benchmark submission. Note that for submissions modeling only a subset of the turbines, the observed and modeled totals are calculated using only the corresponding turbines. Across all submissions, observed data are plotted at 10-minute resolution to increase readability. For the same goal, LES-modeled data are plotted using 2-minute instantaneous values.

465 MAE values in stable conditions in phases 2 and 3 (Figs. S8 and S9), but stable conditions also exhibited higher correlations with observations of power once normalized by inflow turbine productions (Figs. S10 through S15).

A key outcome of this benchmark is the quantification of model improvement enabled by access to additional observations. Figure 19 illustrates the reduction in MAE for participants who submitted results in both phases 1 and 3. Most models achieved lower MAE, with one participant improving by over 40 %. These gains were achieved through distinct strategies detailed in

470 Sect. 3:

- Calibration: Technical University of Munich (FLORIS) and Meteodyn utilized the released wake and SCADA data to calibrate wake decay parameters and tune their models to the specific site conditions.
- Ensemble selection: Equinor (WRF + EWP) refined their ensemble approach by selecting the optimal model member via a cost function that minimized misfit against available SCADA power and lidar wind direction data.
- Resolution and physics: Lawrence Livermore National Laboratory and University of California, Berkeley (WRF-LES) increased model fidelity by moving from two to three nested domains. Similarly, Technical University of Denmark (PyWakeEllipSys) addressed numerical artifacts in the stable case by adopting a modified ABL inflow method. Technical

475

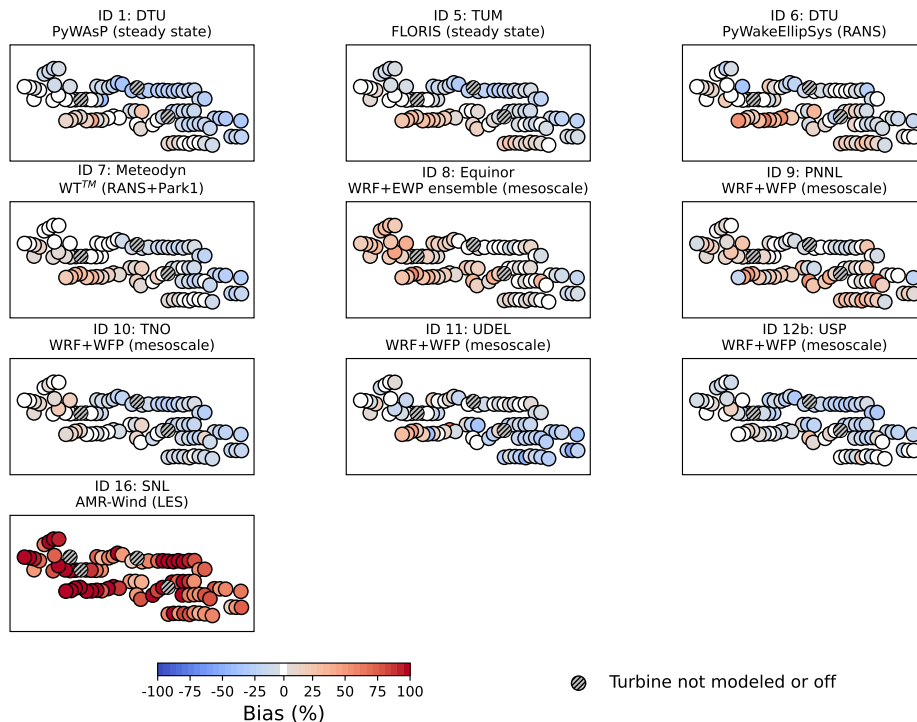


Figure 15. Maps showing the percentage bias in modeled vs. observed power produced by each turbine in the King Plains wind farm on 24 August 2023 for each model submission to Phase 2 of the benchmark.

University of Denmark (PyWASP) improved results by expanding the wind climate input to include multiple lidar data streams.

480 5 Conclusions

The AWAKEN benchmark represents a significant community step for the validation of wind farm flow models, leveraging a uniquely rich dataset to assess model performance across a wide range of fidelities. Beyond a simple comparison of error metrics, this exercise revealed critical insights into the hierarchy of physical drivers governing wind farm performance.

A primary conclusion is that accurate characterization of inflow and terrain effects is as important as accurate wake modeling. The results highlight that increased model complexity does not automatically guarantee improved accuracy. In Phase 1, simpler engineering and steady-state models often matched or outperformed higher-fidelity mesoscale approaches. This counterintuitive result stemmed largely from the boundary condition strategy: simpler models were able to directly ingest the provided in situ inflow observations, whereas mesoscale simulations forced by reanalysis products (e.g., ERA5, HRRR) struggled when the background forcing failed to capture specific atmospheric features, such as the exact timing and height of the nocturnal LLJ or the spatial inhomogeneity of the inflow. Consequently, correctly characterizing the freestream inflow conditions proved

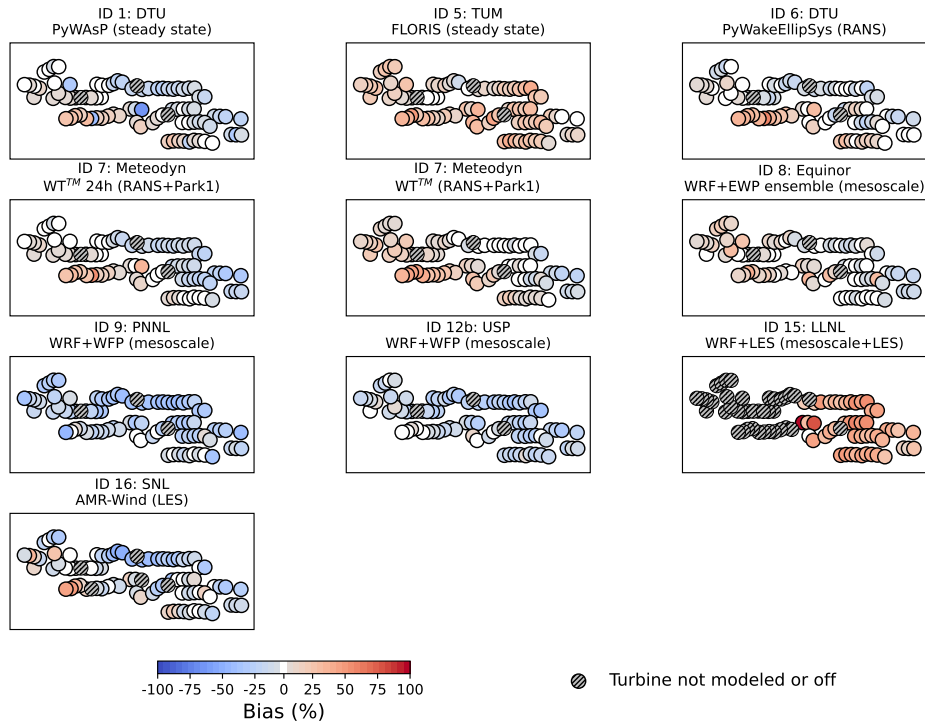


Figure 16. Maps showing the percentage bias in modeled vs. observed power produced by each turbine in the King Plains wind farm on 24 August 2023 for each model submission to Phase 3 of the benchmark.

to be the absolute prerequisite for accurate farm modeling, and more accurate reanalysis products (and mesoscale approaches) would highly contribute to improved wind farm modeling results for simulation tools that require them.

Furthermore, the benchmark underscored the critical role of topography, even in environments often categorized as having simple or moderate terrain. Observational data revealed that terrain-induced flow acceleration frequently outweighed wake losses, causing specific waked turbines to produce more power than those in the inflow row. Most models, regardless of fidelity, struggled to resolve this interplay between the LLJ, wakes, and local terrain-induced speed-ups. This suggests that future modeling efforts must place equal emphasis on microscale terrain resolution as they do on wake parameterization.

The multiphase structure of the benchmark demonstrated that having access to more observations is relatively effective in mitigating these sources of error. As participants gained access to site-specific inflow and wake observations, prediction errors were reduced by up to 40 % in some cases. Persistent challenges remain, particularly in modeling the interaction between atmospheric stability and wake recovery. While models struggle to capture the full temporal variability of wake interactions in unstable conditions, they perform markedly better in stable regimes when inflow variability is reduced.

From a logistical perspective, this exercise provided valuable lessons for future benchmarking initiatives. Clear instructions and standardized data submission templates are essential to ensure consistency across participants and reduce the burden of

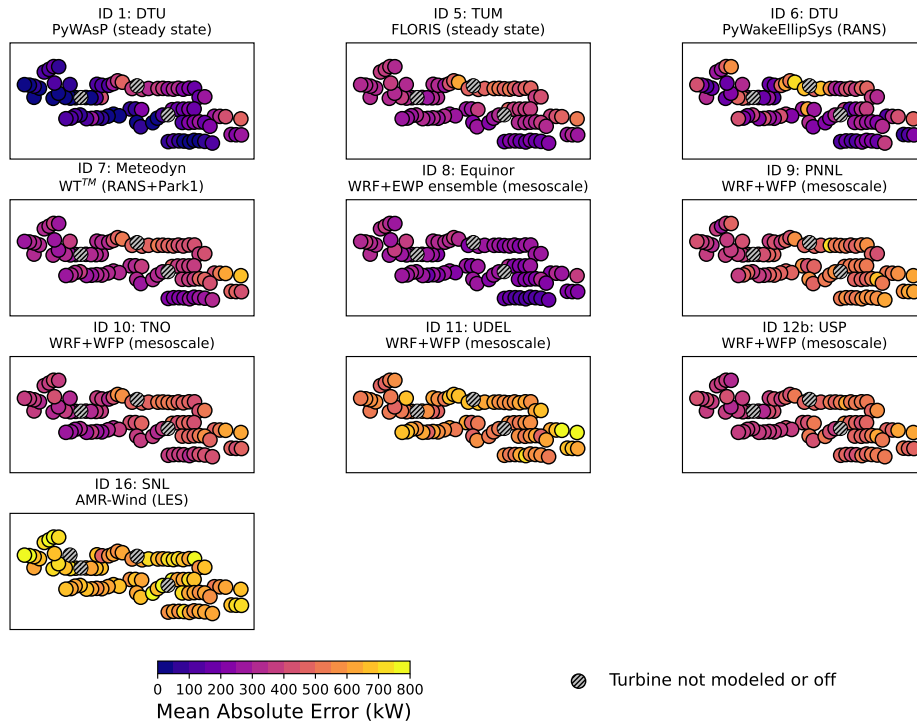


Figure 17. Maps showing the mean absolute error in modeled vs. observed power produced by each turbine in the King Plains wind farm on 24 August 2023 for each model submission to Phase 2 of the benchmark.

505 post-processing. It is also crucial to recognize the constraints of participants; limited time and resources mean that providing massive volumes of observational data does not guarantee it will all be effectively utilized. Finally, scientific priorities vary among research groups. While this benchmark focused on the high-fidelity resolution of single-day flow physics to isolate specific atmospheric phenomena, industry needs often prioritize long-term statistical accuracy. Future work should therefore expand to include long-term benchmarks focused on annual energy production, balancing the need for detailed physical validation with the requirement for statistically representative error quantification over seasonal and annual scales.

510

Data availability. The AWAKEN data released as part of this benchmark are available on Zenodo at <https://doi.org/10.5281/zenodo.15623845> (Bodini et al., 2025).

Author contributions. NB: Conceptualization, Methodology, Formal analysis, Investigation, Validation, Writing - Original Draft. PM: Conceptualization, Funding acquisition, Writing - Review & Editing. RT: Conceptualization, Project administration, Writing - Review & Editing.

515 All authors: Formal analysis, Writing - Review & Editing.

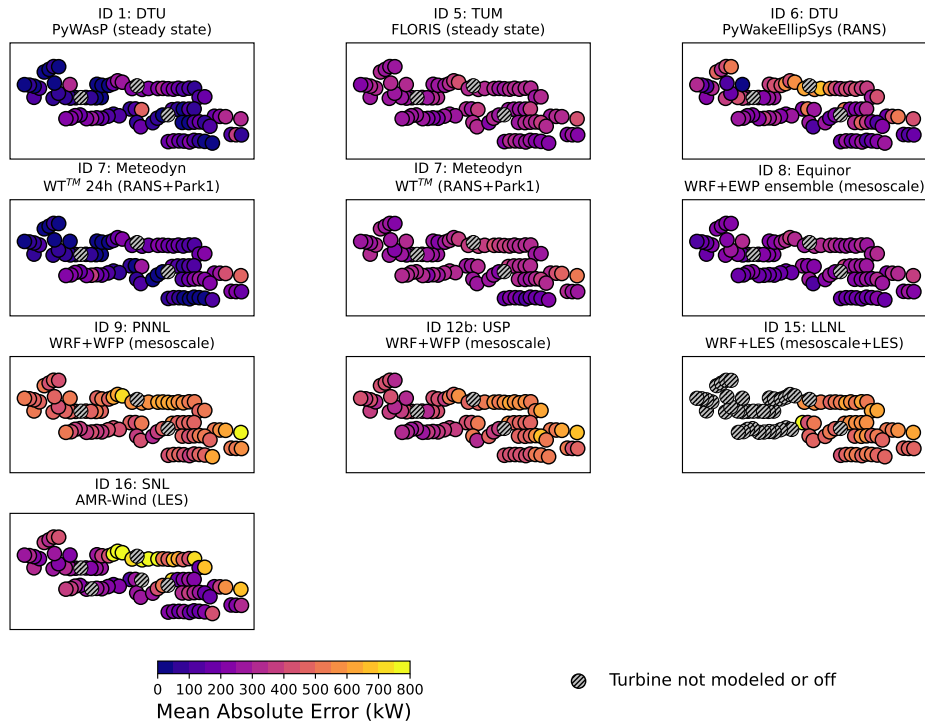


Figure 18. Maps showing the mean absolute error in modeled vs. observed power produced by each turbine in the King Plains wind farm on 24 August 2023 for each model submission to Phase 3 of the benchmark.

Competing interests. A number of (co-)authors are members of the editorial board of *Wind Energy Science*. The authors have no other competing interests to declare.

Acknowledgements. The authors would like to thank ENGIE and GE for agreeing to release proprietary data for the King Plains wind farm to enable the execution of the benchmark.

520 Pacific Northwest National Laboratory is operated for the U.S. Department of Energy (DOE) by the Battelle Memorial Institute under contract DE-AC05-76RL01830.

Additional work was performed under the auspices of the U.S. Department of Energy by Lawrence Livermore National Laboratory under Contract DE-AC52-07NA27344.

525 The work from DTU is partly funded by Independent Research Fund Denmark through the ‘Multi-scale Atmospheric Modeling Above the Seas’ (MAMAS) project (nr. 0217-00055B). It is also partially funded by the Joint Assessment of Models for Wind Energy project (Energy Technology Development and Demonstration Programme project number 134242-521856).

Participants were also partially funded by the European Union Horizon Europe Framework program (HORIZON-CL5-2021-D3-03-04) under grant agreement no. 101084205.

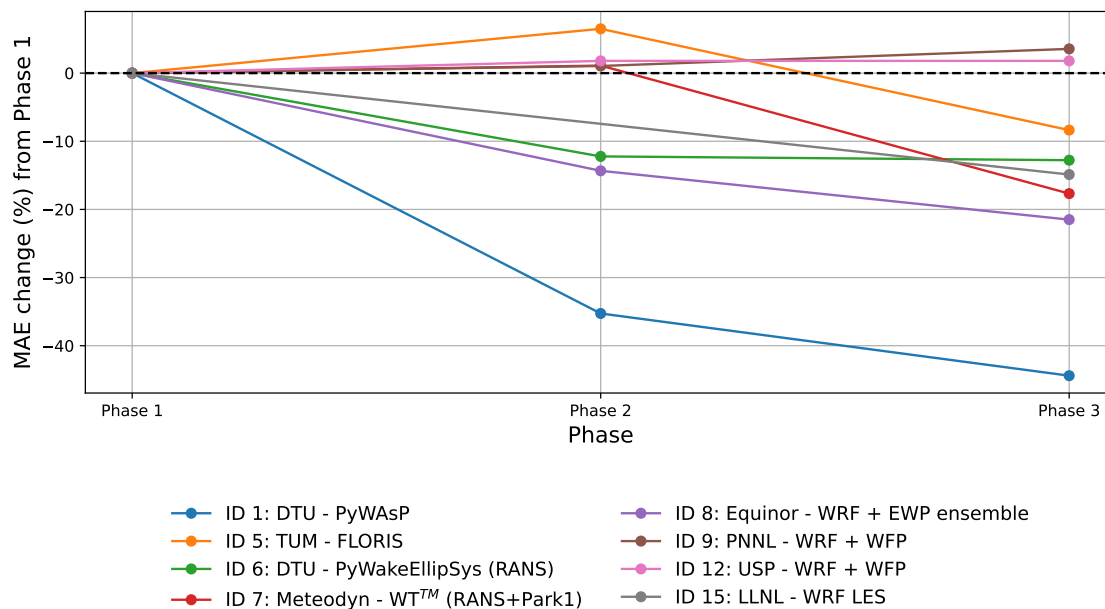


Figure 19. Change in mean absolute error over the different phases of the benchmark for those participants who submitted results in both phases 1 and 3 of the benchmark. Note: the Sandia submission is not included in this plot as each Phase simulated a different period.

A portion of this research was performed using computational resources sponsored by the U.S. Department of Energy’s Office of Critical
 530 Minerals and Energy Innovation and located at the National Laboratory of the Rockies.



References

- Archer, C. L., Wu, S., Ma, Y., and Jiménez, P. A.: Two corrections for turbulent kinetic energy generated by wind farms in the WRF model, *Monthly Weather Review*, 148, 4823–4835, <https://doi.org/10.1175/MWR-D-20-0097.1>, 2020.
- Bastankhah, M. and Porté-Agel, F.: A new analytical model for wind-turbine wakes, *Renewable Energy*, 70, 116–123, <https://doi.org/10.1016/j.renene.2014.01.002>, 2014.
- Bastankhah, M. and Porté-Agel, F.: Experimental and theoretical study of wind turbine wakes in yawed conditions, *Journal of Fluid Mechanics*, 806, 506–541, <https://doi.org/10.1017/jfm.2016.595>, 2016.
- Baungard, M., van der Laan, M. P., and Kelly, M.: RANS modeling of a single wind turbine wake in the unstable surface layer, *Wind Energy Science*, 7, 783–800, <https://doi.org/10.5194/wes-7-783-2022>, 2022a.
- 540 Baungard, M., Van Der Laan, M. P., and Kelly, M.: RANS modeling of a single wind turbine wake in the unstable surface layer, *Wind Energy Science*, 7, 783–800, <https://doi.org/10.5194/wes-7-783-2022>, 2022b.
- Benjamin, S. G., Brown, J. M., Brundage, K. J., Devenyi, D., Grell, G. A., Kim, D., Schwartz, B. E., Smirnova, T. G., Smith, T. L., Weygandt, S. S., and Manikin, G. S.: RUC20: the 20-km version of the Rapid Update Cycle, <https://repository.library.noaa.gov/view/noaa/31413>, last accessed: 2025-12-03, 2002.
- 545 Blondel, F. and Cathelain, M.: An alternative form of the super-Gaussian wind turbine wake model, *Wind Energy Science*, 5, 1225–1236, <https://doi.org/10.5194/wes-5-1225-2020>, 2020.
- Bodini, N., Lundquist, J. K., and Moriarty, P.: Wind plants can impact long-term local atmospheric conditions, *Scientific Reports*, 11, 22 939, <https://doi.org/10.1038/s41598-021-02089-2>, 2021.
- Bodini, N., Abraham, A., Letizia, S., Scott, R., Moriarty, P., and Thedin, R.: AWAKEN wind farm wake benchmark inputs, <https://doi.org/10.5281/zenodo.15623845>, data released as part of the IEA Wind Task 57 JAM benchmark activities, covering all three phases of the exercise. Case study date: 24 August 2023., 2025.
- 550 Bodini, N., Abraham, A., Letizia, S., Lundquist, J. K., Moriarty, P., and Scott, R.: The AWAKEN Wind Farm Benchmark. Part 1: Observed Conditions, *Wind Energy Science*, in review.
- Braunbehrens, R., Vad, A., and Bottasso, C. L.: The wind farm as a sensor: learning and explaining orographic and plant-induced flow heterogeneities from operational data, *Wind Energy Science*, 8, 691–723, <https://doi.org/10.5194/wes-8-691-2023>, 2023.
- 555 Brown, A. R., Hobson, J. M., and Wood, N.: Large-Eddy Simulation Of Neutral Turbulent Flow Over Rough Sinusoidal Ridges, *Boundary-Layer Meteorology*, 98, 411–441, <https://doi.org/10.1023/A:1018703209408>, 2001.
- Chen, F. and Dudhia, J.: Coupling an advanced land surface–hydrology model with the Penn State–NCAR MM5 modeling system. Part I: Model implementation and sensitivity, *Monthly weather review*, 129, 569–585, [https://doi.org/10.1175/1520-0493\(2001\)129<0569:CAALSH>2.0.CO;2](https://doi.org/10.1175/1520-0493(2001)129<0569:CAALSH>2.0.CO;2), 2001.
- 560 Crespo, A. and Hernández, J.: Turbulence characteristics in wind-turbine wakes, *Journal of Wind Engineering and Industrial Aerodynamics*, 61, 71–85, [https://doi.org/10.1016/0167-6105\(95\)00033-X](https://doi.org/10.1016/0167-6105(95)00033-X), 1996.
- Deardorff, J. W.: Stratocumulus-capped mixed layers derived from a three-dimensional model, *Boundary-layer meteorology*, 18, 495–527, <https://doi.org/10.1007/BF00119502>, 1980.
- 565 Doubrava, P., Quon, E. W., Martinez-Tossas, L. A., Shaler, K., Debnath, M., Hamilton, N., Herges, T. G., Maniaci, D., Kelley, C. L., Hsieh, A. S., Blaylock, M. L., van der Laan, P., Andersen, S. J., Krueger, S., Cathelain, M., Schlez, W., Jonkman, J., Branlard, E., Steinfeld, G.,



- Schmidt, S., Blondel, F., Lukassen, L. J., and Moriarty, P.: Multimodel validation of single wakes in neutral and stratified atmospheric conditions, *Wind Energy*, 23, 2027–2055, <https://doi.org/https://doi.org/10.1002/we.2543>, 2020.
- Dowell, D. C., Alexander, C. R., James, E. P., Weygandt, S. S., Benjamin, S. G., Manikin, G. S., Blake, B. T., Brown, J. M., Olson, J. B.,
570 Hu, M., Smirnova, T. G., Ladwig, T., Kenyon, J. S., Ahmadov, R., Turner, D. D., Duda, J. D., and Alcott, T. I.: The High-Resolution Rapid Refresh (HRRR): An hourly updating convection-allowing forecast model. Part I: Motivation and system description, *Weather and Forecasting*, 37, 1371–1395, <https://doi.org/10.1175/WAF-D-21-0151.1>, 2022.
- DTU Wind and Energy Systems: PyWakeEllipSys v5.4, https://topfarm.pages.windenergy.dtu.dk/cuttingedge/pywake/pywake_ellipsys/, 2025.
- 575 Dudhia, J.: Numerical study of convection observed during the winter monsoon experiment using a mesoscale two-dimensional model, *Journal of Atmospheric Sciences*, 46, 3077–3107, [https://doi.org/10.1175/1520-0469\(1989\)046<3077:NSOCOD>2.0.CO;2](https://doi.org/10.1175/1520-0469(1989)046<3077:NSOCOD>2.0.CO;2), 1989.
- Ferry, M.: New features of the MIGAL solver, in: *Proceedings of the PHOENICS Users International Conference*, Moscow, 2002.
- Fitch, A. C., Olson, J. B., Lundquist, J. K., Dudhia, J., Gupta, A. K., Michalakes, J., and Barstad, I.: Local and mesoscale impacts of wind farms as parameterized in a mesoscale NWP model, *Monthly Weather Review*, 140, 3017–3038, <https://doi.org/10.1175/MWR-D-11-00352.1>, 2012.
580
- Floors, R., Badger, M., Troen, I., Grogan, K., and Permien, F.-H.: Satellite-based estimation of roughness lengths and displacement heights for wind resource modelling, *Wind Energy Science*, 6, 1379–1400, <https://doi.org/10.5194/wes-6-1379-2021>, 2021.
- Floors, R., Troen, I., and Peña, A.: Using observed and modelled heat fluxes for improved extrapolation of wind distributions, *Boundary-Layer Meteorology*, 188, 75–101, <https://doi.org/10.1007/s10546-023-00803-3>, 2023.
- 585 Frandsen, S.: Turbulence and turbulence-generated structural loading in wind turbine clusters, Risø-R Report Risø-R-1188(EN), Risø National Laboratory, Roskilde, Denmark, ISBN 978-87-550-3458-7, https://backend.orbit.dtu.dk/ws/files/12674798/ris_r_1188.pdf, 2007.
- Hersbach, H., Bell, B., Berrisford, P., Hirahara, S., Horányi, A., Muñoz-Sabater, J., Nicolas, J., Peubey, C., Radu, R., Schepers, D., Simmons, A., Soci, C., Abdalla, S., Abellan, X., Balsamo, G., Bechtold, P., Biavati, G., Bidlot, J., Bonavita, M., De Chiara, G., Dahlgren, P., Dee, D., Diamantakis, M., Dragani, R., Flemming, J., Forbes, R., Fuentes, M., Geer, A., Haimberger, L., Healy, S., Hogan, R. J., Hólm, E.,
590 Janisková, M., Keeley, S., Laloyaux, P., Lopez, P., Lupu, C., Radnoti, G., de Rosnay, P., Rozum, I., Vamborg, F., Villaume, S., and Thépaut, J.-N.: The ERA5 global reanalysis, *Quarterly journal of the royal meteorological society*, 146, 1999–2049, <https://doi.org/10.1002/qj.3803>, 2020.
- Hong, S.-Y., Noh, Y., and Dudhia, J.: A new vertical diffusion package with an explicit treatment of entrainment processes, *Monthly weather review*, 134, 2318–2341, <https://doi.org/10.1175/MWR3199.1>, 2006.
- 595 Janjić, Z. I.: The step-mountain eta coordinate model: Further developments of the convection, viscous sublayer, and turbulence closure schemes, *Monthly Weather Review*, 122, 927–945, 1994.
- Jensen, N. O.: A note on wind generator interaction, Risø National Laboratory, 1983.
- Katic, I., Højstrup, J., and Jensen, N. O.: A Simple Model for Cluster Efficiency, in: *EWEC’86. Proceedings*, edited by Palz, W. and Sesto, E., vol. 1, pp. 407–410, A. Raguzzi, https://backend.orbit.dtu.dk/ws/files/106427419/A_Simple_Model_for_Cluster_Efficiency_EWEC_86_.pdf, accessed: 2025-12-03, 1987.
600
- Khanjari, A. and Archer, C.: A framework for the superposition of wind turbines wake properties, *Wind Energy Science Discussions*, 2025, 1–29, <https://doi.org/10.5194/wes-2025-220>, 2025.
- Khanjari, A., Feroz, A., and Archer, C.: An analytical formulation for turbulent kinetic energy added by wind turbines based on large-eddy simulation, *Wind Energy Science*, 10, 887–905, <https://doi.org/10.5194/wes-10-887-2025>, 2025.



- 605 Kuhn, M. B., Henry de Frahan, M. T., Mohan, P., Deskos, G., Churchfield, M., Cheung, L., Sharma, A., Almgren, A., Ananthan, S., Brazell, M. J., Martínez-Tossas, L. A., Thedin, R., Rood, J., Sakievich, P., Vijayakumar, G., Zhang, W., and Sprague, M.: AMR-Wind: A Performance-Portable, High-Fidelity Flow Solver for Wind Farm Simulations, *Wind Energy*, 28, e70010, <https://doi.org/10.1002/we.70010>, 2025.
- Ma, Y., Archer, C. L., and Vassel-Be-Hagh, A.: Comparison of individual versus ensemble wind farm parameterizations inclusive of sub-grid
610 wakes for the WRF model, *Wind Energy*, 25, 1573–1595, <https://doi.org/10.1002/we.2758>, 2022.
- Mellor, G. L. and Yamada, T.: Development of a turbulence closure model for geophysical fluid problems, *Reviews of Geophysics*, 20, 851–875, <https://doi.org/10.1029/RG020i004p00851>, 1982.
- Michelsen, J. A.: Basis3D—a Platform for Development of Multiblock PDE Solvers: β -release, 1992.
- Mirocha, J. D., Kosovic, B., Aitken, M. L., and Lundquist, J. K.: Implementation of a generalized actuator disk wind turbine model into the
615 weather research and forecasting model for large-eddy simulation applications, *Journal of Renewable and Sustainable Energy*, 6, 013 104, <https://doi.org/10.1063/1.4861061>, 2014.
- Mlawer, E. J., Taubman, S. J., Brown, P. D., Iacono, M. J., and Clough, S. A.: Radiative transfer for inhomogeneous atmospheres: RRTM, a validated correlated-k model for the longwave, *Journal of Geophysical Research: Atmospheres*, 102, 16 663–16 682, <https://doi.org/10.1029/97JD00237>, 1997.
- 620 Morrison, H. and Milbrandt, J.: Comparison of two-moment bulk microphysics schemes in idealized supercell thunderstorm simulations, *Monthly Weather Review*, 139, 1103–1130, <https://doi.org/10.1175/2010MWR3433.1>, 2011.
- Nakanishi, M. and Niino, H.: Development of an improved turbulence closure model for the atmospheric boundary layer, *Journal of the Meteorological Society of Japan. Ser. II*, 87, 895–912, <https://doi.org/10.2151/jmsj.87.895>, 2009.
- NREL: FLORIS: Wind farm flow modeling software, <https://github.com/NREL/floris>, accessed: 2025-05-09, 2024.
- 625 Nygaard, N. G., Poulsen, L., Svensson, E., and Pedersen, J. G.: Large-scale benchmarking of wake models for offshore wind farms, *Journal of Physics: Conference Series*, 2265, 022 008, <https://doi.org/10.1088/1742-6596/2265/2/022008>, 2022.
- Pedersen, J. G., Svensson, E., Poulsen, L., and Nygaard, N. G.: Turbulence Optimized Park model with Gaussian wake profile, *Journal of Physics: Conference Series*, 2265, 022 063, <https://doi.org/10.1088/1742-6596/2265/2/022063>, 2022.
- Pedersen, M. M., Forsting, A. M., van der Laan, P., Riva, R., Alcayaga Román, L. A., Criado Risco, J., Friis-Møller, M., Quick, J.,
630 Schøler Christiansen, J. P., Valotta Rodrigues, R., Olsen, B. T., and Réthoré, P.-E.: PyWake 2.5.0: An open-source wind farm simulation tool, <https://gitlab.windenergy.dtu.dk/TOPFARM/PyWake>, software, DTU Wind, Technical University of Denmark, 2023.
- Peña, A., Mirocha, J. D., and van der Laan, M. P.: Evaluation of the Fitch wind-farm wake parametrization with large-eddy simulations of wakes using the Weather Research and Forecasting model, *Mon. Weather Rev.*, 150, 3051–3064, 2022.
- 635 Peña, A. and Mirocha, J. D.: One-year-long turbulence measurements and modeling using large-eddy simulation domains in the Weather Research and Forecasting model, *Applied Energy*, 363, 123 069, 2024.
- Pope, S. B.: *Turbulent Flows*, Cambridge University Press, Cambridge, 2000.
- Quick, J., rsmouradi, Schulte, J., mathieu7an, DTUplaa, Olsen, B. T., and ernie: EUFLOW/WIFA: v0.1.0, <https://doi.org/10.5281/zenodo.17058703>, 2025.
- 640 Radünz, W. C., Carmo, B., Lundquist, J. K., Letizia, S., Abraham, A., Wise, A. S., Sanchez Gomez, M., Hamilton, N., Rai, R. K., and Peixoto, P. S.: Influence of simple terrain on the spatial variability of a low-level jet and wind farm performance in the AWAKEN field campaign, *Wind Energy Science*, 10, 2365–2393, <https://doi.org/10.5194/wes-10-2365-2025>, 2025.



- Schøler, J. P., Simutis, E., van der Laan, M. P., Quick, J., and Réthoré, P.-E.: Validation of RANS-calibrated engineering models and ANN-based surrogate for wind farm flow simulation and layout optimization, submitted to Wind Energy Science, 2026.
- 645 Sørensen, N. N.: General purpose flow solver applied to flow over hills, 1995.
- Thompson, G., Field, P. R., Rasmussen, R. M., and Hall, W. D.: Explicit forecasts of winter precipitation using an improved bulk microphysics scheme. Part II: Implementation of a new snow parameterization, Monthly weather review, 136, 5095–5115, <https://doi.org/10.1175/2008MWR2387.1>, 2008.
- Troen, I. and Petersen, E. L.: European Wind Atlas, Risø National Laboratory, 1989.
- 650 Troldborg, N. and Meyer Forsting, A. R.: A simple model of the wind turbine induction zone derived from numerical simulations, Wind Energy, 20, 2011–2020, <https://doi.org/10.1002/we.2137>, 2017.
- van der Laan, M. P., Kelly, M., Baungaard, M., and Dicholkar, A.: A simple steady-state inflow model of the neutral and stable atmospheric boundary layer applied to wind turbine wake simulations, Wind Energy Science, 9, 1985–2000, <https://doi.org/10.5194/wes-9-1985-2024>, 2024.
- 655 van der Laan, M. P., Paraskevopoulos, I., and Kelly, M.: A damping method for RANS wind farm flow simulations subjected to shallow atmospheric boundary layers, Journal of Physics: Conference Series, 3016, 012 001, <https://doi.org/10.1088/1742-6596/3016/1/012001>, 2025.
- van der Laan, M. P., Centurelli, G., Steinfeld, G., and Musaddiq, H.: On the connection between wind veer and numerical waves in steady-state atmospheric wind farm simulations, Submitted to Torque, 2026.
- 660 Volker, P. J., Badger, J., Hahmann, A. N., and Ott, S.: The Explicit Wake Parametrisation V1. 0: a wind farm parametrisation in the mesoscale model WRF, Geoscientific Model Development, 8, 3715–3731, <https://doi.org/10.5194/gmd-8-3715-2015>, 2015.
- Vollmer, L., Sengers, B. A. M., and Dörenkämper, M.: Brief communication: A simple axial induction modification to the Weather Research and Forecasting Fitch wind farm parameterization, Wind Energy Science, 9, 1689–1693, <https://doi.org/10.5194/wes-9-1689-2024>, 2024.
- Wise, A. S., Arthur, R. S., Abraham, A., Wharton, S., Krishnamurthy, R., Newsom, R., Hirth, B., Schroeder, J., Moriarty, P., and Chow, F. K.: Large-eddy simulation of an atmospheric bore and associated gravity wave effects on wind farm performance in the southern Great Plains, Wind Energy Science, 10, 1007–1032, <https://doi.org/10.5194/wes-10-1007-2025>, 2025.
- Wong, V. and Lilly, D. K.: A comparison of two dynamic subgrid closure methods for turbulent thermal convection, Physics of Fluids, 6, 1016–1023, <https://doi.org/10.1063/1.868335>, 1994.